

Article

# New 8-Hydroxyquinoline-Bearing Quinoxaline Derivatives as Effective Corrosion Inhibitors for Mild Steel in HCl: Electrochemical and Computational Investigations

Abdelkarim Chaouiki <sup>1</sup>, Maryam Chafiq <sup>1</sup>, Mohamed Rbaa <sup>2</sup>, Hassane Lgaz <sup>3</sup>, Rachid Salghi <sup>1</sup>, Brahim Lakhrissi <sup>2</sup>, Ismat H. Ali <sup>4</sup>, Sheerin Masroor <sup>5</sup> and Youngjae Cho <sup>6,\*</sup>

- <sup>1</sup> Laboratory of Applied Chemistry and Environment, ENSA, University Ibn Zohr, PO Box 1136, Agadir 80000, Morocco; abdelkarim.chaouiki@uit.ac.ma (A.C.); maryam.chafiq@edu.uiz.ac.ma (M.C.); r.salghi@uiz.ac.ma (R.S.)
- <sup>2</sup> Laboratory of Organic Chemistry, Catalysis and Environment, Faculty of Sciences, Ibn Tofail University, P.O. Box 133, Kenitra 14000, Morocco; mohamed.rbaa10@gmail.com (M.R.); b.lakhrissi2012@gmail.com (B.L.)
- <sup>3</sup> Department of Crop Science, College of Sanghur Life Science, Konkuk University, Seoul 05029, Korea; hlgaz@konkuk.ac.kr
- <sup>4</sup> Department of Chemistry, College of Science, King Khalid University, P. O. Box 9004, Abha 61413, Saudi Arabia; ismathassanali@gmail.com
- <sup>5</sup> Department of Chemistry, Anugrah Narayan College, Patliputra University, Patna 800013, India; masroor.sheerin@gmail.com
- <sup>6</sup> Department of Food Science and Technology, Pusan National University, 1268-50 Samrangjin-ro, Samrangjin-eup, Miryang 50463, Korea
- \* Correspondence: moonjaeworld@naver.com; Tel.: +82-2-450-3048; Fax: +82-2-455-3726

Received: 4 August 2020; Accepted: 19 August 2020; Published: 21 August 2020



**Abstract:** There has been substantial research undertaken on the role of green synthesized corrosion inhibitors as a substantial approach to inhibit the corrosion of metals and their alloys in acidic environments. Herein, electrochemical studies, surface characterization, and theoretical modeling were adopted to investigate the corrosion inhibition proprieties of novel synthesized quinoxaline derivatives bearing 8-Hydroxyquinoline, namely 1-((8-hydroxyquinolin-5-yl)methyl)-3,6-dimethylquinoxalin-2(1H)-one (Q1) and 1-((8-hydroxyquinolin-5-yl)methyl) quinoxalin-2(1H)-one (Q2) on mild steel corrosion in 1 mol/L HCl solution. The principal finding of this research was that both inhibitors acted as good corrosion inhibitors with Q1 having the highest performance (96% at  $5 \times 10^{-3}$  mol/L). Electrochemical results obtained via potentiodynamic polarization (PDP) and electrochemical impedance spectroscopy (EIS) techniques demonstrated that quinoxaline compounds belonged to mixed-type inhibitors; their presence significantly increased the polarization resistance, preventing simultaneously anodic and cathodic reactions. Further, experimental results provided preliminary insights about the interactions mode between studied molecules and the mild steel surface, which followed the Langmuir adsorption model, and physical and chemical interactions assisted their inhibition mechanism. Besides, SEM analyses confirmed the existence of protective film on the metal surface after the addition of  $5 \times 10^{-3}$  mol/L of quinoxalines. In addition, the temperature and immersion time effects on inhibition performances of quinoxalines were investigated to evaluate their performances in different operating conditions. Besides, Density Functional Theory (DFT) and molecular dynamics (MD) simulations were carried out to explore the most reactive sites of quinoxaline inhibitors and their interaction mechanism. Theoretical results revealed that the inhibitor molecule with additional electron-donating functional group strongly interacted with the steel surface.

**Keywords:** corrosion inhibition; mild steel; quinoxaline; SEM; quantum chemical calculation; MD simulations

---

## 1. Introduction

Corrosion in its general definition results from chemical or electrochemical action of an environment on metals and alloys in contact [1]. The consequences are important in various fields and, in particular, in the oil and gas industry, which in many cases, reduces its production or even needs to replace the corroded materials [2]. Iron and its alloys are, therefore, materials of choice for use in the industrial field thanks to their mechanical properties. However, steel, like all metals, is subject to all forms of corrosion. Commonly referred to as inorganic acid solutions, for instance, HCl, HNO<sub>3</sub>, H<sub>2</sub>SO<sub>4</sub>, and others can be found in a variety of industrial applications [3,4]. Hydrochloric acid is one of the best choices for acid treatment (acidizing) in oil and gas production because of its immense value in improving the productivity (stimulation) of wells. It has been used for many years to increase the injectivity and initial productivity of new wells or restoring inactive wells [5]. Corrosion is a major problem in environments containing acidic solutions. In this case, the use of organic corrosion inhibitors is one of the simplest, most effective and practical methods of preventing corrosion by reducing the serious adverse effects on metal surfaces [6]. However, the selection of corrosion inhibitors that are safe and effective enough to protect iron and its alloys has become a challenge to engineers and researchers. With all these considerations in mind, it would appear need at this stage a selection of environmentally friendly, cost-effective inhibitors with high inhibition efficiency and ease of synthesis and use [7].

On the other hand, organic compounds with high inhibitory efficacy should contain heteroatoms such as nitrogen, sulfur, oxygen, along with other special characteristics [8]. Among organic families that can meet these specific requirements, we find quinoxalines. Much research papers have been produced on quinoxaline derivatives. For example, Inqui [9] has been tested as a mild steel corrosion inhibitor with a concentration of  $10 \times 10^{-6}$  mol/L and showed an inhibition efficiency of about 82%. This study showed that compounds tested in the paper are effective inhibitors against mild steel corrosion in HCl media and that their effective adsorption protects the metal in the test medium. Additionally, the corrosion behavior of steel in HCl has been studied using 2-phenylthieno (3, 2-b) quinoxaline [10], which shows efficiency of about 95%. The authors reported that inhibition of quinoxaline derivatives increased with increasing inhibitor concentration, and their adsorption follows isotherm model. In another research, two derivatives named Q1 and Q2 were synthesized and tested as corrosion inhibitors of copper in 2 mol/L HNO<sub>3</sub> and showed high inhibition properties in this environment [11]. Fu et al. [12], in their full article on quinoxalines, give an idea of the type of adsorption involved by the four derivatives, which all have been acted as mixed-type inhibitors. In that paper, the authors also used theoretical studies to explore the most reactive site of quinoxaline compounds and their adsorption mechanism on the Fe surface. On the other hand, 8-hydroxyquinoline derivatives have been proven to be a source of highly effective corrosion inhibitors of metals and alloys in various operating conditions [13–16].

With this in mind, the objective of the current paper is to study in depth the influence that can make the addition of 8-Hydroxyquinoline moiety on the corrosion inhibition properties of two quinoxalines, namely 1-((8-hydroxyquinolin-5-yl)methyl)-3,6-dimethylquinoxalin-2(1H)-one (Q1) and 1-((8-hydroxyquinolin-5-yl)methyl)quinoxalin-2(1H)-one (Q2) for MS corrosion in 1.0 mol/L HCl solution (hereafter, compounds will be abbreviated as quinoxaline derivatives). Our initial hypothesis is that the presence of several reactive sites (heteroatoms and conjugated systems) in both quinoxaline and 8-Hydroxyquinoline moieties could ensure high adsorption on the metal surface and thus preventing the spread of corrosion. Therefore, this study's key focus is to assess and discuss the ability of compounds under study to be potent inhibitors of MS corrosion in acidic solutions. The assessment of inhibition performance in this study is accomplished experimentally using weight loss, electrochemical

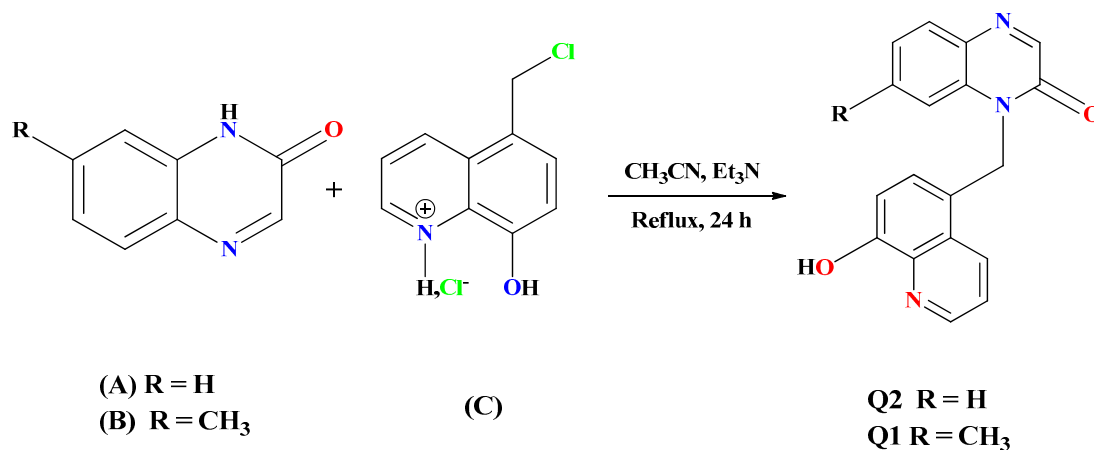
and SEM methods. Quantum chemical calculations by DFT were also performed to correlate the efficacy of the studied compounds with molecular electronic properties. As well, an investigation of the adsorption capacity of corrosion inhibitors that could account for the experimental results was examined using simulation calculations, namely MD modeling and radial distribution function (RDF). Combining both experimental and theoretical investigations, the results of this study is expected to generate considerable outcomes that could clarify the adsorption behavior and inhibition mechanism of investigated quinoxaline derivatives.

## 2. Experimental Sections

### 2.1. Synthesis of Compounds

All products and materials used for the synthesis of these compounds were purchased from the company Sigma Aldrich.

**Synthesis of 1-((8-hydroxyquinolin-5-yl) methyl)-6-alkylquinoxalin-2 (1H)-ones:** This synthesis was carried out by condensation of 6-alkylquinoxalin-2 (1H)-ones (A,B) with 5-chloromethyl 8-hydroxyquinoline hydrochloride (C) in acetonitrile (CH<sub>3</sub>CN) in the presence of triethylamine (Et<sub>3</sub>N) at reflux for 24 h (Scheme 1).



**Scheme 1.** Synthesis of 1-((8-hydroxyquinolin-5-yl) methyl)-6-alkylquinoxalin-2 (1H)-ones.

**General procedure for the synthesis of 1-((8-hydroxyquinolin-5-yl) methyl)-6-alkylquinoxalin-2 (1H)-ones (Q1 and Q2):** 0.01 mole of 6-alkylquinoxaline-2,3 (1H, 4H) -dione (A and B) is mixed with 0.02 mol of 5-chloromethyl-8-hydroxyquinoline hydrochloride (C) in 50 mL of acetonitrile (CH<sub>3</sub>CN) in the presence of 0.03 mol of triethylamine (Et<sub>3</sub>N). The reaction mixture is brought to reflux with magnetic stirring for 24 h. The reaction is monitored by TLC using a mixture of hexane/dichloromethane (4:6, v/v) as eluent. The reaction mixture is concentrated on a rotary evaporator under a water pump vacuum. The organic phases are combined, washed with water saturated with NaCl, dried over anhydrous magnesium sulfate (MgSO<sub>4</sub>) and concentrated to dryness on a rotary evaporator under a water pump. The crude residue obtained is purified by chromatography on a silica gel column using a mixture of hexane/dichloromethane (4:6, v/v) as eluent, followed by recrystallization from a DMSO-EtOH mixture (3/7) (Scheme 1). Full characterization of both compounds has been reported in the Supplementary Material (Scheme S1, Figure S1).

### 2.2. Materials and Solution

Mild steel (MS), type AISI 1018 with elemental composition of (in wt.%): 0.19 C, 0.20 Si, 0.81 Mn, 0.0027 S, 0.12 Cr, 0.001 P, 0.11 Ni, 0.18 Cu, 0.032 Al, and balance Fe is the material tested in the present paper. The electrolyte is a solution prepared from a 37% HCl solution of the brand Sigma-Aldrich, and it

was used to prepare acidic environment at a concentration of 1.0 mol/L by diluting it with distilled water. Although a higher concentration is used in practical applications, in this study, 1.0 mol/L was used as a representative concentration of hydrochloric acid corrosion to avoid severe deterioration of the exposed mild steel surface, while 303 K was set as ambient temperature, in accordance with similar studies reported in the literature [17,18]. MS specimens were mechanically polished before use at the beginning of each test by using a rotating disc with the abrasive paper of increasingly fine grain size from SiC 400, 800, 1200 up to 1600. After that, the steel samples under study were successively degreased in acetone; they were rinsed with distilled water, dried and transferred immediately for conducting the experimental analysis. After preliminary tests, various concentrations viz.  $5 \times 10^{-3}$ ,  $1 \times 10^{-3}$ ,  $5 \times 10^{-4}$  and  $1 \times 10^{-4}$  mol/L of Q1 and Q2 inhibitors were prepared to carry out different experimental methods. The anti-corrosion effect of studied inhibitors on mild steel corrosion has been analyzed, evaluated, and then compared with uninhibited solutions.

### 2.3. Weight Loss and Electrochemical Measurements

The weight loss method was performed under ASTM G 31–72 standard methodology [16]. The MS specimens were immersed for 24 h in blank and inhibited solutions in the absence of agitation and maintained at different temperatures ranging from 303 to 333 K. After the required time, mild steel specimens were retrieved from test solutions, and corrosion products were removed by a pickling acid solution, then washed by distilled water and acetone and dried before reweighing them again by using a Metler balance. To increase the reliability of measures, each test was carried out in triplicate. The inhibition efficiency value given is the average of three tests conducted under the same conditions for each concentration. The following Equation (1) was used to estimate the corrosion rate of mild steel:

$$C_R = \frac{K \times W}{A \times t \times \rho} \quad (1)$$

where  $K$  is a constant equal to  $8.76 \times 10^4$ ,  $t$  is the time of exposure in hours,  $W$  is the mass loss in gram,  $\rho$  is the density of used steel and equal to  $7.86 \text{ g cm}^{-3}$  [19]. The exposed surface area,  $A$  (in  $\text{cm}^2$ ) was calculated from Equation (2) [20]:

$$A = \frac{\pi}{2}(D^2 - d^2) + l\pi D + l\pi d \quad (2)$$

where  $D$ ,  $d$ , and  $l$  are the diameter of mild steel pieces, the diameter of the hole for holding and the thickness, respectively.

The inhibition efficiency of both inhibitors was calculated using Equation (3):

$$\eta_{WL}(\%) = \left[ 1 - \frac{C_R}{C_R} \right] 100 \quad (3)$$

where  $C_R$  and  $C_R$  are respectively the values of corrosion rates in blank and inhibited solutions.

For electrochemical experiments, a Volta lab potentiostat/galvanostat (Wuhan Corrtest Instruments Corp., Wuhan, China) and monitored by electrochemical analyzer software was used. The electrochemical experiments were done using a double-walled cell equipped with a thermometer (Scheme S2, Supplementary Material). The three electrodes of the used electrochemical cell are: an electrode type that is saturated calomel as the reference electrode, a platinum wire as auxiliary or counter electrode and the working electrode is a mild steel coupon placed close to the reference electrode. Mild steel sample of rectangular shape was coated with epoxy resin, leaving  $1 \text{ cm}^2$  exposed to the electrolyte. To achieve the stabilization of the system, the MS electrode was immersed in the test solution containing 80 mL of corrosive solution for 30 min at open circuit potential (OCP) [18]. The electrochemical impedance experiments were performed in the frequency range of 10 mHz to 100 kHz by superimposing a sinusoidal AC signal of small amplitude, 5 mV, at the open circuit potential.

EC-lab software was used to extract and simulate the EIS data. The polarization resistances were used to estimate the inhibition performance according to the following formula:

$$\eta_{EIS}(\%) = \left[ \frac{R_p^i - R_p}{R_p^i} \right] 100 \quad (4)$$

where  $R_p$  and  $R_p^i$  are respectively, the polarization resistance with and without inhibitors.

The potentiodynamic polarization measurements were conducted by sweeping the electrode potential in the range of  $-700$  to  $-300$  mV versus  $E_{OCP}$  with a sweep rate of  $0.16 \text{ mV s}^{-1}$ . Electrochemical parameters like corrosion potential ( $E_{corr}$ ), Tafel slopes and corrosion current density ( $i_{corr}$ ) were estimated from Tafel curves. The inhibition efficiency of studied inhibitors was calculated using  $i_{corr}$  and defined as bellow:

$$\eta_{PDP}(\%) = \left[ \frac{i_{corr} - i_{corr}^i}{i_{corr}} \right] 100 \quad (5)$$

where  $i_{corr}$  and  $i_{corr}^i$  indicates respectively the corrosion current density with and without inhibitors.

## 2.4. Theoretical Evaluation

### 2.4.1. DFT Details

To get more details about electronic properties of the corrosion inhibitor molecules and their effect on the adsorption mechanism during corrosion process, quantum chemical calculations were evaluated and discussed in detail. Conceptual Density Functional Theory (CDFT) that is related to the chemical reactivity of atoms, ions and molecules is an important branch of DFT. In this study, the geometry optimization of studied compounds and the calculation of quantum chemical parameters have been obtained by Gaussian software Ver. 09W using B3LYP method with 6-311G++(d,p) basis set [21]. Firstly, the quinoxaline derivatives under study were thoroughly analyzed, and the optimized structure is used to extract some useful theoretical parameters. By these calculations, the frontier molecular orbitals such as the energy of the highest occupied molecular orbital ( $E_{HOMO}$ ) and energy of lowest unoccupied molecular orbital ( $E_{LUMO}$ ) were estimated by applying the Koopmans' theorem [22]. Koopmans Theorem known as an alternative way proposed for the prediction of ionization energy and electron affinity values of molecules states that "ionization energy and electron affinity of a molecule correspond to the negative values of its HOMO and LUMO orbital energies, respectively". Additionally, the energy gap ( $\Delta E$ ) can be estimated using the values of  $E_{HOMO}$  and  $E_{LUMO}$ , from which the electronegativity and the global hardness can also be determined. All these descriptors are calculated using the following Equations [23]:

$$IP = -E_{HOMO} \quad (6)$$

$$EA = -E_{LUMO} \quad (7)$$

$$\chi = \frac{IP + EA}{2} \quad (8)$$

$$\eta = \frac{IP - EA}{2} \quad (9)$$

$$\Delta E = E_{LUMO} - E_{HOMO} = IP - EA \quad (10)$$

Moreover, considering the work function ( $\phi$ ) instead of the electronegativity of metal, the Pearson method was used to calculate the fraction of electrons transferred ( $\Delta N$ ), according to the following formula [24,25]:

$$\Delta N = \frac{\phi_{Fe} - \chi_{inh}}{2(\eta_{Fe} - \eta_{inh})} \quad (11)$$

where  $\emptyset$  is the work function ( $\varphi_{\text{Fe}} = 4.82$  eV for the F (110) plan), whereas the global hardness of iron is neglected because  $\eta$  of bulk metals is related to the inverse of their density of states at the Fermi level, which is an exceedingly small number [26].

#### 2.4.2. Local Reactivity: FUKUI Functions

Understanding local reactivity of inhibitor molecules can help us gain insight into the adsorption mechanism of inhibitor molecules in a more precise way [27]. For this purpose, Fukui functions indices were determined with the aid of DMol<sup>3</sup> as a reliable module integrated into the Materials Studio 6.0 program using generalized gradient first principles approximation (GGA) and Perdew, Burke and Ernzerhof formalism known as PBE with double numerical basis sets plus polarization (DNP) [28,29] in the COSMO implicit solvent model [30]. By using some important mathematical approaches, the condensed Fukui functions of the molecules were estimated to discuss the ability of each atom in the molecule for electrophilic and nucleophilic attacks. Fukui functions were determined based on the finite difference approximation using Hirshfeld Population Analysis (HPA) via the following equations [31]:

$$f_k^+ = q_k(N+1) - q_k(N) \quad (12)$$

$$f_k^- = q_k(N) - q_k(N-1) \quad (13)$$

where  $q_k(N)$ ,  $q_k(N+1)$ , and  $q_k(N-1)$  refer to the atomic charges of neutral, anionic and cationic species, respectively.

#### 2.4.3. Molecular Dynamic Simulations

One of the most well-known tools for assessing the adsorption behavior of inhibitor molecule on metal surfaces is molecular dynamics (MD) simulations. In this study, the adsorption of investigated inhibitors on the iron surface was simulated by performing MD modeling using Forcite calculations, amorphous construction as well as the Build layer modules implemented in Materials Studio 6.0 program. For all of the studied system, the Fe (110) surface with a slab of 15 Å is picked up because it was found to have high stabilization energy and a highly packed structure compared to other iron planes, i.e., Fe (111) and Fe (101) [32]. Further details with more information about the interaction process between the inhibitor molecule and Fe (110) surface for each simulation by using MD modeling was explained elsewhere [33–36]. Furthermore, inhibitor/metal interactions, which could be elucidated by interaction and binding energies, were evaluated when the studied systems reach their equilibrium state. For this, the interaction energy, as well as binding energy, was calculated using Equations (14) and (15) [37]:

$$E_{\text{interaction}} = E_{\text{total}} - (E_{\text{surface}+\text{H}_2\text{O}+\text{H}_3\text{O}^++\text{Cl}^-}) \quad (14)$$

$$E_{\text{binding}} = E_{\text{interaction}} \quad (15)$$

where  $E_{\text{total}}$ ,  $E_{\text{surface}+\text{H}_2\text{O}+\text{H}_3\text{O}^++\text{Cl}^-}$ ,  $E_{\text{inhibitor}}$  are the single point energies for all system, Fe(110) surface including H<sub>2</sub>O, H<sub>3</sub>O<sup>+</sup>, and Cl<sup>-</sup> ions and the inhibitor molecule alone, respectively.

#### 2.4.4. Radial Distribution Function (RDF)

It is important to explore a very important aspect of the molecular proprieties and their intermolecular interactions. For this purpose, further investigations are required to shed light on the interaction type underlying when an inhibitor molecule adsorbs on the iron surface. To this end, radial distribution function (RDF) analysis computed from simulation trajectories is an important tool to capture the complexities of the adsorption phenomenon on the metallic surface. In the present work, the RDF,  $g(r)$ , is defined as the probability of finding particle B within the range around particle

A. The following formula is used for the calculation of RDF, which is proposed by Hansen and McDonald [38].

$$g(r) = \frac{1}{\langle \rho_B \rangle_{local}} \times \frac{1}{N_A} \sum_{i \in A} \sum_{j \in B} \frac{\delta(r_{ij} - r)}{4\pi r^2} \tag{16}$$

where  $\langle \rho_B \rangle_{local}$  represents the particle density of B average over all shells beside particle A. The theory of RDF has been addressed in detail by Hansen and McDonald [38].

### 2.5. SEM Analysis

The surface characteristics of corroded and inhibited MS samples were investigated by scanning electron microscope (SEM, Hitachi TM-1000, Hitachi, Ltd., Tokyo, Japan). Before SEM analysis, the MS samples were exposed to uninhibited and inhibited solutions for 24 h. The specimen’s surface experienced a similar pre-treatment, as explained earlier in weight loss tests.

## 3. Results and Discussion

### 3.1. Weight Loss Tests: Influence of Concentration and Temperature on Inhibition Efficiency

Experiments of weight loss were conducted over 24 h in both without and with the use of several concentrations of quinoxaline derivatives being tested at different temperatures. In Figure 1, results for corrosion rate and inhibition efficiency derived based on the weight loss tests were reported. By using a higher concentration of corrosion inhibitor, the effectiveness of the inhibition is increased, whereas, on the other hand, the corrosion rate is reduced. Moreover, a considerably reduced corrosion rate is achieved under the same conditions with increasing inhibitor concentration. The highest inhibitory performance was achieved when  $5 \times 10^{-3}$  mol/L was added, whereas there was almost insignificant growth with higher concentrations of both compounds. Results provide data indicating that both quinoxaline derivatives showed a high degree of inhibition under the proposed conditions. The difference noticed regarding efficacy between the two investigated molecules might be understood as a function of the electron-donating ability of the studied quinoxalines. These data and their relationship to the molecular structure of each compound will be discussed in detail in the succeeding paragraphs.

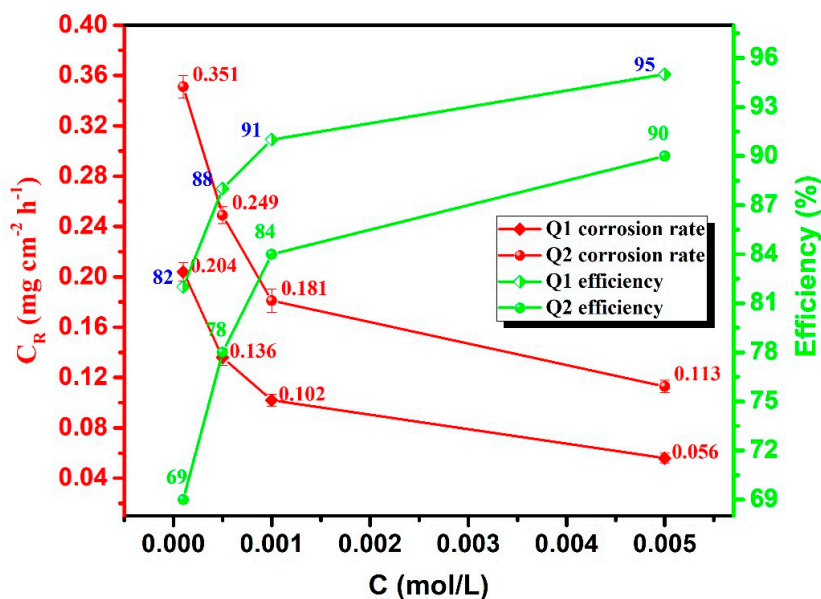
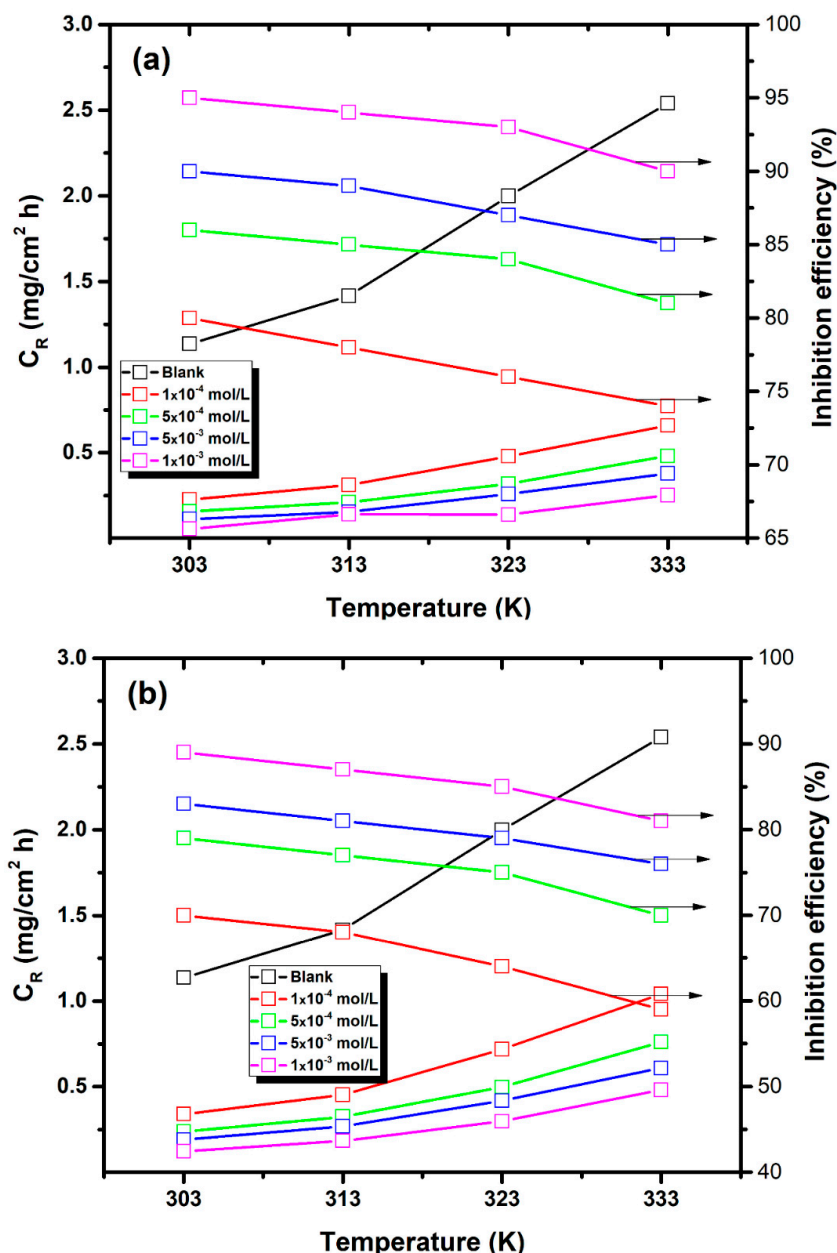


Figure 1. The variation of the corrosion rate ( $\pm$ SD) and the inhibition efficiency with Q1 and Q2 concentrations for mild steel in 1.0 M HCl at 303 K.

As part of this work, the effect of temperature on efficacy was investigated using variable temperatures ranging from 303 to 333 K at an optimum concentration. Indeed, as a result of the anodic corrosion process in acidic solutions, ions of metal leave the metallic surface into solution. In contrast, in the cathodic corrosion process, hydrogen ions are discharged to produce hydrogen gas. This process takes place rapidly with the increase of the temperature, which is considered one of the factors influencing the speed of the chemical reactions [39]. Based on Figure 2, as the temperature increases, it is obvious that the corrosion rate increases while the value of the inhibition efficiency is considerably decreasing. This behavior is well noted for both compounds.



**Figure 2.** The effect of temperature toward the corrosion rate and inhibition efficiency for MS without and with (a) Q1 and (b) Q2.

### 3.2. Potentiodynamic Polarization Curves

This part of this study seeks to understand, on the one hand, the dynamics of metal corrosion and explain, on the other hand, the influence of quinoxaline derivatives on the corrosion kinetics of mild

steel dissolution. Figure 3 shows the polarization curves of MS electrode in 1.0 mol/L HCl solution at 303 K without and with different concentrations of Q1 and Q2 compounds. The corrosion parameters such as corrosion potential ( $E_{\text{corr}}$ ), anodic and cathodic Tafel slopes and corrosion current density ( $i_{\text{corr}}$ ) were obtained by extrapolation of the Tafel lines. The said parameters, as well as inhibition efficiency of inhibitors under study, are listed in Table 1. The results of this investigation (Figure 3) show that the presence of Q1 and Q2 inhibitors results in a marked influence on both cathodic and anodic curves toward lower corrosion current densities. This indicates that the surface of MS is affected by the addition of each inhibitor, meaning that they can retard iron oxidation and  $\text{H}^+$  reduction during cathodic and anodic reactions.

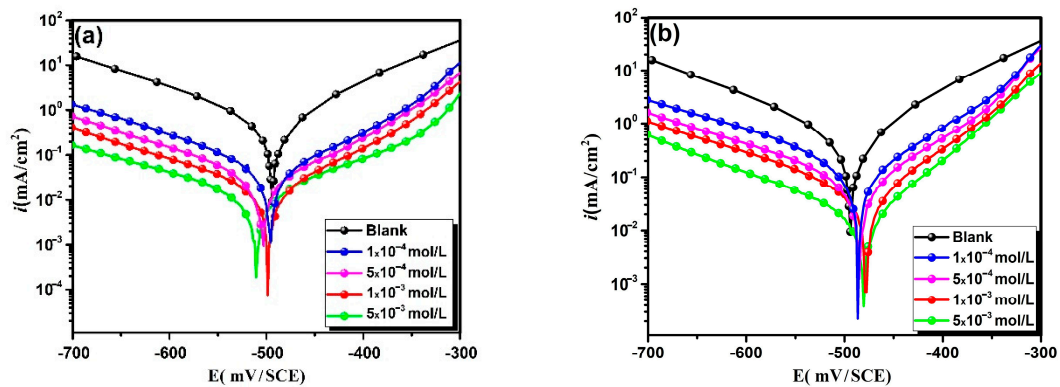


**Figure 3.** PDP curves of mild steel corrosion in the absence and presence of various concentrations of (a) Q1 and (b) Q2 at 303 K.

**Table 1.** Polarization parameters and inhibition efficiency of MS in 1 mol/L HCl solution without and with different concentrations of Q1 and Q2 at 303 K.

Inhibitor	Concentration (mol/L)	$-E_{\text{corr}}$ (mV vs. SCE)	$-\beta_c$ (mV dec $^{-1}$ )	$-\beta_a$ (mV dec $^{-1}$ )	$i_{\text{corr}}$ ( $\mu\text{A cm}^{-2}$ )	$\eta_{\text{PDP}}$ (%)
	1.0	496 $\pm$ 0.4	150 $\pm$ 3.5	92 $\pm$ 5.7	564 $\pm$ 2.3	-
Q1	1 $\times$ 10 $^{-4}$	498 $\pm$ 0.9	143 $\pm$ 5.4	101 $\pm$ 6.4	112 $\pm$ 2.5	80
	5 $\times$ 10 $^{-4}$	506 $\pm$ 0.7	146 $\pm$ 4.3	98 $\pm$ 2.7	78 $\pm$ 3.2	86
	1 $\times$ 10 $^{-3}$	500 $\pm$ 0.4	140 $\pm$ 3.1	99 $\pm$ 4.9	56 $\pm$ 1.8	90
	5 $\times$ 10 $^{-3}$	513 $\pm$ 0.8	168 $\pm$ 3.2	84 $\pm$ 5.4	25 $\pm$ 2.1	95
	1 $\times$ 10 $^{-4}$	491 $\pm$ 1.7	163 $\pm$ 5.7	93 $\pm$ 1.5	169 $\pm$ 3.3	70
Q2	5 $\times$ 10 $^{-4}$	487 $\pm$ 2.2	175 $\pm$ 6.6	75 $\pm$ 2.8	118 $\pm$ 4.4	79
	1 $\times$ 10 $^{-3}$	480 $\pm$ 0.9	166 $\pm$ 4.1	73 $\pm$ 6.8	95 $\pm$ 3.2	83
	5 $\times$ 10 $^{-3}$	483 $\pm$ 2.3	140 $\pm$ 5.7	66 $\pm$ 5.3	62 $\pm$ 2.1	89

At the same time, it can be observed that the corrosion potential values moved slightly towards the cathode in the case of Q1, while  $E_{\text{corr}}$  moved slightly around a more positive path parallel to the blank in the presence of Q2. Much of the available literature on the adsorption mechanism of inhibitors deals with the question regarding the nature of inhibitor molecules, i.e., during the corrosion process, are the investigated compounds work as cathodic, anodic or mixed type inhibitors? Based on the values of displacement of  $E_{\text{corr}}$  of inhibited solutions in comparison with the blank solution, an inhibitor can be regarded as anodic or cathodic type inhibitor if the displacement of  $E_{\text{corr}}$  is larger than 85 mV, while the  $E_{\text{corr}}$  shift less than 85 mV could be attributed to the mixed character of the inhibitor [40,41]. In the present work, we noted that the values of corrosion potential did not vary drastically and the displacement is lower than 85 mV, verifying that the Q1 and Q2 worked as mixed-type inhibitors. Furthermore, from Figure 3 and Table 1 it can be seen that, with the addition of compounds under study, the variation in the values of anodic and cathodic Tafel slopes is small. The polarization curves of Q1 and Q2 show parallel trends, confirming that the anodic dissolution of MS along with

hydrogen evolution reactions are controlled without changing the mechanism of the corrosion process. Another important result is that the values of  $i_{\text{cor}}$  decreased, and inhibition performance increased with the addition of Q1 and Q2 compounds (via Table 1). The highest inhibition performance observed at the concentration of  $5 \times 10^{-3}$  mol/L is of 95% for Q1 as the most effective inhibitor, then 89% for Q2 at the same concentration. This reflects the effect of quinoxaline compounds on corrosion inhibition in acidic medium facilitated by the presence of heteroatoms present in polar functional groups like hydroxyl ( $-\text{OH}$ ) as well as the existence of  $\pi$ -electrons and unsaturated functional groups like  $> \text{C} = \text{O}$ . It is worth mentioning that the higher inhibition performance marked in the case of Q1 inhibitor could be attributed to the presence of two  $\text{CH}_3$  as electron-donating groups, which are expected to enhance electron density on the molecule and thus effectively adsorbed on the steel surface.

### 3.3. EIS Measurements

#### 3.3.1. Concentration Effect

Before performing each experimental procedure, open-time potential ( $E_{\text{ocp}}$ ) tests were conducted in the 1.0 mol/L HCl solutions in the absence and presence of the two inhibitors (Figure S2, Supplementary Material). An electrical equivalent circuit model (EEC) is essential to analyze and simulate experimental results. The EEC model used in present work (Figure S3, Supplementary Material) consists of the polarization resistance of the interface of the MS/electrolyte, a solution resistance, and a constant phase element (CPE). The CPE was employed instead of a pure capacitor, which is affected by imperfections of the surface. In Figure 4, the Nyquist and Bode diagrams of MS in 1.0 mol/L hydrochloric acid alone and one containing various concentrations of inhibitors at 303 K are represented.

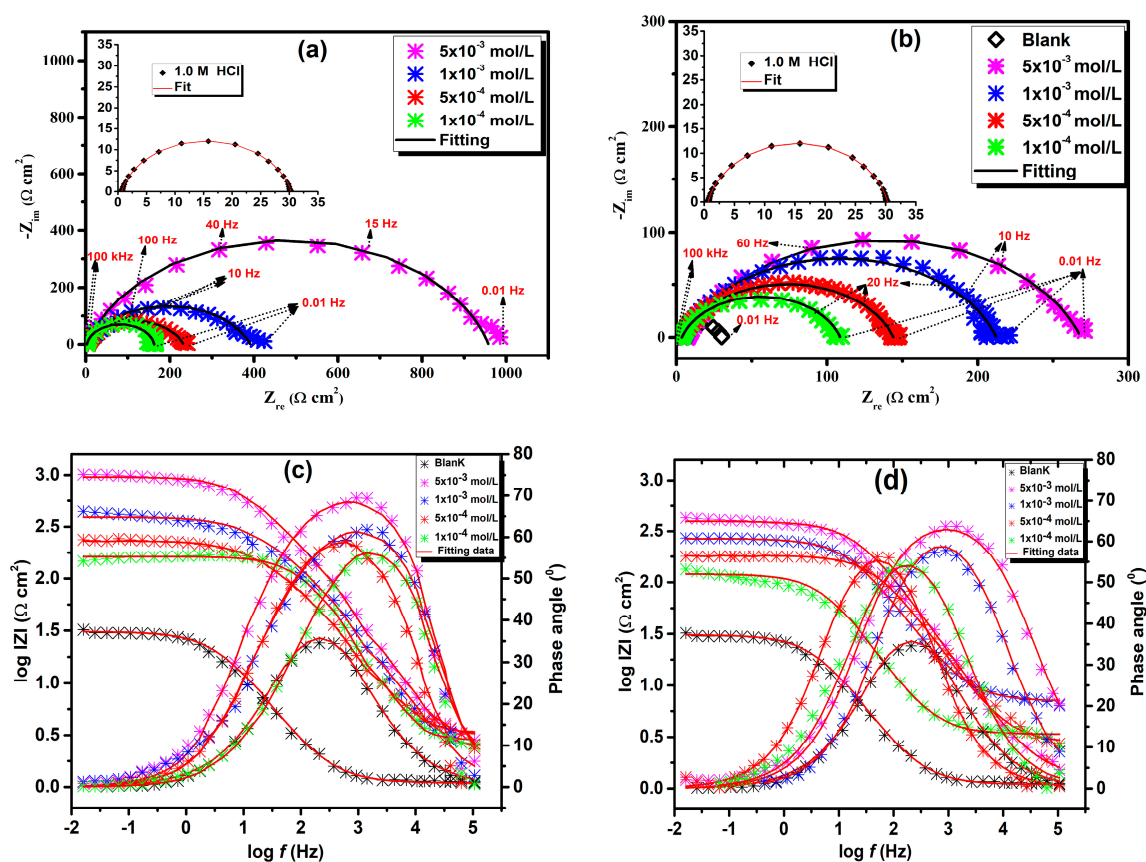


**Figure 4.** Nyquist and Bode plots for mild steel corrosion in 1.0 M HCl without and with different inhibitors concentrations of Q1 and Q2, (a) Nyquist plots of Q1, (b) Nyquist plots of Q2, (c) Bode plots of Q1, (d) Bode plots of Q2.

In an uninhibited solution, the Nyquist plots measured in HCl solution is a recessed capacitive loop. In contrast, the semicircular diameter of the plots becomes larger as the concentration of inhibitor rises. Spectra of impedance measurements have not displayed half-ideal circles generally linked to ideal capacitors. Thus, extreme phase angle values are not shown to exceed ( $-70^\circ$ ) in the phase angle plots. The obtained results are grouped in Table 2. For each case, the double-layer electrical capacity ( $C_{dl}$ ) is calculated based on the following equation [42]:

$$C_{dl} = \sqrt[n]{QR_p^{1-n}} \quad (17)$$

where  $n$  gives the phase shift that enables the calculation of the surface heterogeneity of mild steel.

**Table 2.** Impedance parameters and inhibition efficiency values for MS in HCl medium in uninhibited and inhibited solutions at 303 K.

Inhibitor	Concentration (mol/L)	$R_p$ ( $\Omega \text{ cm}^2$ )	$n$	$Q \times 10^{-4}$ ( $\text{S}^n \Omega^{-1} \text{ cm}^{-2}$ )	$C_{dl}$ ( $\mu\text{F cm}^{-2}$ )	Goodness of fit ( $\chi^2$ ) $\times 10^{-3}$	$\eta_{\text{EIS}}$ (%)
	1.0	$29 \pm 1.5$	$0.89 \pm 0.005$	$1.761 \pm 0.0025$	92	0.33	-
Q1	$1 \times 10^{-4}$	$160 \pm 1.7$	$0.80 \pm 0.007$	$0.7319 \pm 0.0047$	24	2.85	81
	$5 \times 10^{-4}$	$229 \pm 1.3$	$0.79 \pm 0.009$	$0.6171 \pm 0.0076$	19	3.29	87
	$1 \times 10^{-3}$	$389 \pm 1.8$	$0.81 \pm 0.005$	$0.4092 \pm 0.0077$	15	2.33	92
	$5 \times 10^{-3}$	$954 \pm 1.4$	$0.82 \pm 0.006$	$0.2478 \pm 0.0066$	10	2.52	96
Q2	$1 \times 10^{-4}$	$105 \pm 1.8$	$0.79 \pm 0.001$	$1.0115 \pm 0.0035$	30	3.64	72
	$5 \times 10^{-4}$	$140 \pm 1.9$	$0.81 \pm 0.004$	$0.7055 \pm 0.0045$	24	3.47	79
	$1 \times 10^{-3}$	$208 \pm 1.4$	$0.79 \pm 0.007$	$0.6102 \pm 0.0094$	19	4.26	85
	$5 \times 10^{-3}$	$267 \pm 1.6$	$0.80 \pm 0.003$	$0.5144 \pm 0.0024$	17	3.01	89

As can be seen from the EIS data in Table 2, for both inhibitor molecules, when the concentration of inhibitors increases,  $R_p$  values are also increased. Besides, a decrease in the double layer capacity ( $C_{dl}$ ) occurs as a result of an increase in double-layer thickness [43,44].

### 3.3.2. Immersion Time Effect

To have a clearer view of the mechanism of these quinoxaline derivatives, in addition to the effects of concentration and temperature on inhibition, the effect of immersion time is studied. The choice of the  $5 \times 10^{-3}$  mol/L concentration is justified because at this concentration, the efficiency is maximal. Based on the EIS technique, the inhibitory behavior of a quinoxaline derivative is monitored after 30 min, 6, 12 and 24 h of immersion, as shown in Figure 5.

All the extracted parameters are grouped in Table 3. As shown in the table, it can be seen that the polarization resistance of mild steel in the presence of the inhibitor under investigation decreases as the immersion time increases. The stable film formation is a function of time and since polarization resistance tends to decrease, the adsorbed inhibitor starts to desorb with the increase in immersion time [45,46]. Besides, almost a stable value of the inhibiting efficiency as the immersion time increases is noticed. The stable inhibition efficiency at longer immersion time is reasonable due to the accompanied decrease in polarization resistance of the metal over time. A decrease in the  $C_{dl}$  value can be seen, which due to the blocking of the active sites for corrosive dissolution by inhibitor's molecules, thus forming a protective layer on the MS surface.

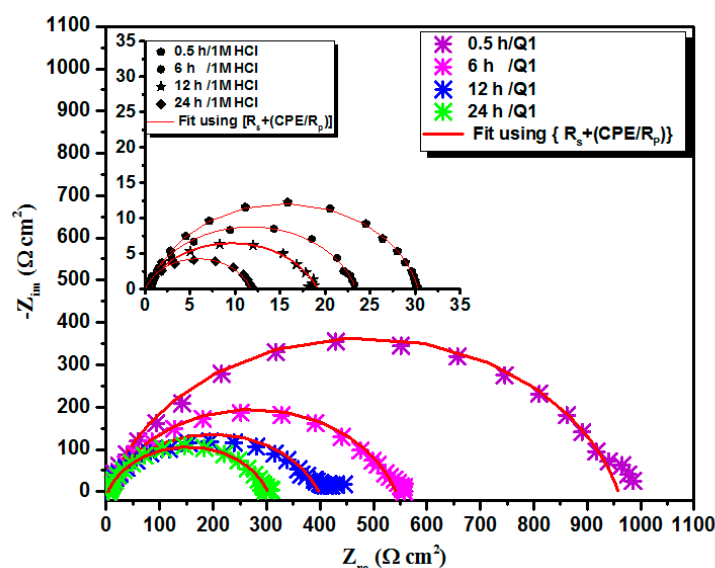


**Figure 5.** EIS plots of MS substrate immersed in uninhibited and inhibited solution at 303 K containing  $5 \times 10^{-3}$  M of Q1 at varied times.

**Table 3.** Effect of immersion time on polarization resistance and inhibition efficiency of MS in the absence and presence of Q1.

Inhibitor	Time (h)	$R_p$ ( $\Omega\text{cm}^2$ )	$n$	$Q \times 10^{-4}$ ( $\text{S}^n \Omega^{-1} \text{cm}^{-2}$ )	$C_{dl}$ ( $\mu\text{F cm}^2$ )	Goodness of fit ( $\chi^2 \times 10^{-3}$ )	$\eta_{EIS}$ (%)
Q1	0.5	$29 \pm 1.5$	$0.89 \pm 0.005$	$1.7610 \pm 0.0025$	92	0.33	-
	6	$23 \pm 2.5$	$0.84 \pm 0.007$	$2.5114 \pm 0.0037$	94	2.45	-
	12	$18 \pm 1.7$	$0.83 \pm 0.004$	$2.9866 \pm 0.0084$	102	3.24	-
	24	$12 \pm 2.9$	$0.88 \pm 0.003$	$3.0891 \pm 0.0031$	144	1.14	-
	0.5	$954 \pm 1.4$	$0.82 \pm 0.006$	$0.2478 \pm 0.0066$	10	1.79	96
	6	$537 \pm 1.8$	$0.83 \pm 0.007$	$0.3787 \pm 0.0075$	17	2.03	95
	12	$395 \pm 1.5$	$0.82 \pm 0.003$	$0.5176 \pm 0.0023$	22	1.28	95
	24	$300 \pm 2.1$	$0.81 \pm 0.005$	$0.6754 \pm 0.0078$	27	3.16	96

### 3.4. Adsorption Isotherm

Further research needs to examine more closely the links between the protection performance of inhibitors and their adsorption phenomenon. As indicated in the previous parts of this manuscript, the nature of the interaction between investigated inhibitors and MS surface has mainly occurred through adsorption processes. For this purpose, adsorption isotherms were fitted to explore more insight into the adsorption model of Q1 and Q2 compounds on mild steel surface as well as the thermodynamic parameters. In this regard, different adsorption isotherm models, including Langmuir, Freundlich, Frumkin and Flory-Huggins, have been tested (Figure S4, Supplementary Material). To fit different adsorption isotherms, the values of  $\theta$  (degree of surface coverage) were derived from weight loss measurements. The fitting results obtained by Langmuir adsorption isotherm model are displayed in Figure S5 (Supplementary Material). Looking at the fitted plots presented in Figure S5, it can be seen that the greatest fit was identified for the Langmuir adsorption isotherm model delineated by the following equation [47]:

$$\frac{C}{\theta} = \frac{1}{K_{ads}} + C \tag{18}$$

in which C denotes the concentration of Q1 and Q2 and  $K_{ads}$  stands for adsorptive equilibrium constant.

As Figure S5 shows, plots of  $(C/\theta)$  versus (C) are linear with good correlation coefficients ( $R^2 = 0.999$ ) and slopes values equal to unity, indicating that the adsorption of Q1 and Q2 on the surface of the steel in 1.0 mol/L HCl media at all temperatures obeys the Langmuir adsorption model. To judge the

adsorption type of Q1 and Q2 on the steel surface, the free energy of adsorption ( $\Delta G_{\text{ads}}^0$ ) of the inhibitor is calculated using Equation (19). It can be noted that the ( $\Delta G_{\text{ads}}^0$ ) of inhibitor is directly related to the  $K_{\text{ads}}$  which is obtained from the intercepts in Figure S5.

$$\Delta G_{\text{ads}}^0 = -RT \ln(55.5K_{\text{ads}}) \quad (19)$$

where  $R$  = universal gas constant ( $8.314 \text{ J K}^{-1} \text{ mol}^{-1}$ ) and  $T$  = absolute temperature.

Based on the Langmuir model, the calculated parameters are shown in Table 4. From these results, it found that the  $K_{\text{ads}}$  values for Q1 and Q2, computed from graphs' intercepts, are quite high, reflecting the important adsorption ability of Q1 and Q2 molecules on the MS surface. More so, it is clear that  $K_{\text{ads}}$  of Q1 (26,752 L/mol at 303 K) is higher than that of Q2 (14009 L/mol at 303 K) of the same family. This could be due to the better adsorption of Q1 molecule on the MS surface and thus providing high corrosion inhibition performance. Table 4 also shows that calculated values of adsorption free energy  $\Delta G_{\text{ads}}^0$  are negative and are between  $-34$  and  $-38 \text{ kJ/mol}$  at all temperatures. The negative sign of  $\Delta G_{\text{ads}}^0$  indicates that the adsorption of inhibitors on the metal is a spontaneous process. Additionally, the estimated values of  $\Delta G_{\text{ads}}^0$  confirmed that the adsorption of both inhibitors in aqueous 1.0 mol/L HCl belongs to a combined type of physical and chemical adsorption. Generally, as mentioned in the literature review [48,49],  $\Delta G_{\text{ads}}^0 \sim -40 \text{ kJ mol}^{-1}$  or more negative demonstrates chemisorption type,  $\Delta G_{\text{ads}}^0 \sim -20 \text{ kJ mol}^{-1}$  or less negative signifies that the adsorption is a physical process, whereas mixed type adsorption is identified when  $\Delta G_{\text{ads}}^0$  are between  $-20$  and  $-40 \text{ kJ mol}^{-1}$ .

**Table 4.** The adsorption parameters for the corrosion of MS in inhibited solutions at different temperatures.

Inhibitor	Q1				Q2			
	303 K	313 K	323 K	333 K	303 K	313 K	323 K	333 K
Temperature	303 K	313 K	323 K	333 K	303 K	313 K	323 K	333 K
Slope	1.04	1.02	1.03	1.02	1.06	1.03	1.04	1.04
$K_{\text{ads}} (\text{M}^{-1})$	26,752	20,312	18,102	18,533	14,009	14,604	13,524	12,289
$\Delta G_{\text{ads}}^0 (\text{KJ mol}^{-1})$	-35.78	-36.24	-37.09	38.30	-34.15	-35.38	-36.31	-37.17

### 3.5. Surface Analysis

The influence of quinoxaline derivatives under study on the morphology of mild steel surface as well as the observation of the electrode surfaces was performed and evaluated using a scanning electron microscope. The SEM analyses were done on the MS surface before and after immersion in the aggressive solution for 24 h at 303 K in the absence and presence of quinoxaline compounds. Figure 6a–d shows the images of the surface of a fresh abraded mild steel surface and surface of MS specimens retrieved from 1.0 mol/L HCl solutions before and after addition of  $5 \times 10^{-3} \text{ mol/L}$  of Q1 and Q2 inhibitors. By identifying the differences between SEM micrographs of all treated surfaces, we can get an insight into the capacity of tested corrosion inhibitors in protecting the metal surface. Before immersion, as shown in Figure 6a, the surface of the freshly abraded MS sample is uniform along with the presence of some marks of polishing and abrasions.

In contrast, after immersion in 1.0 mol/L HCl alone, the corrosion attack of the mild steel surface is very serious. Figure 6b displays a large damaged surface area, and some areas of localized corrosion could be seen, which is due to acid attack. Thus, the mild steel surface is highly susceptible towards damage from acid attack in absence of inhibitors. Compared to the samples placed in inhibited solutions, the positive impact of investigated molecules on the corrosion inhibition of mild steel is significantly marked. It can be seen from Figure 6c that the corrosion attack on the mild steel surface became significantly smaller in the presence of inhibitor and almost a smoother and uniform surface is achieved.

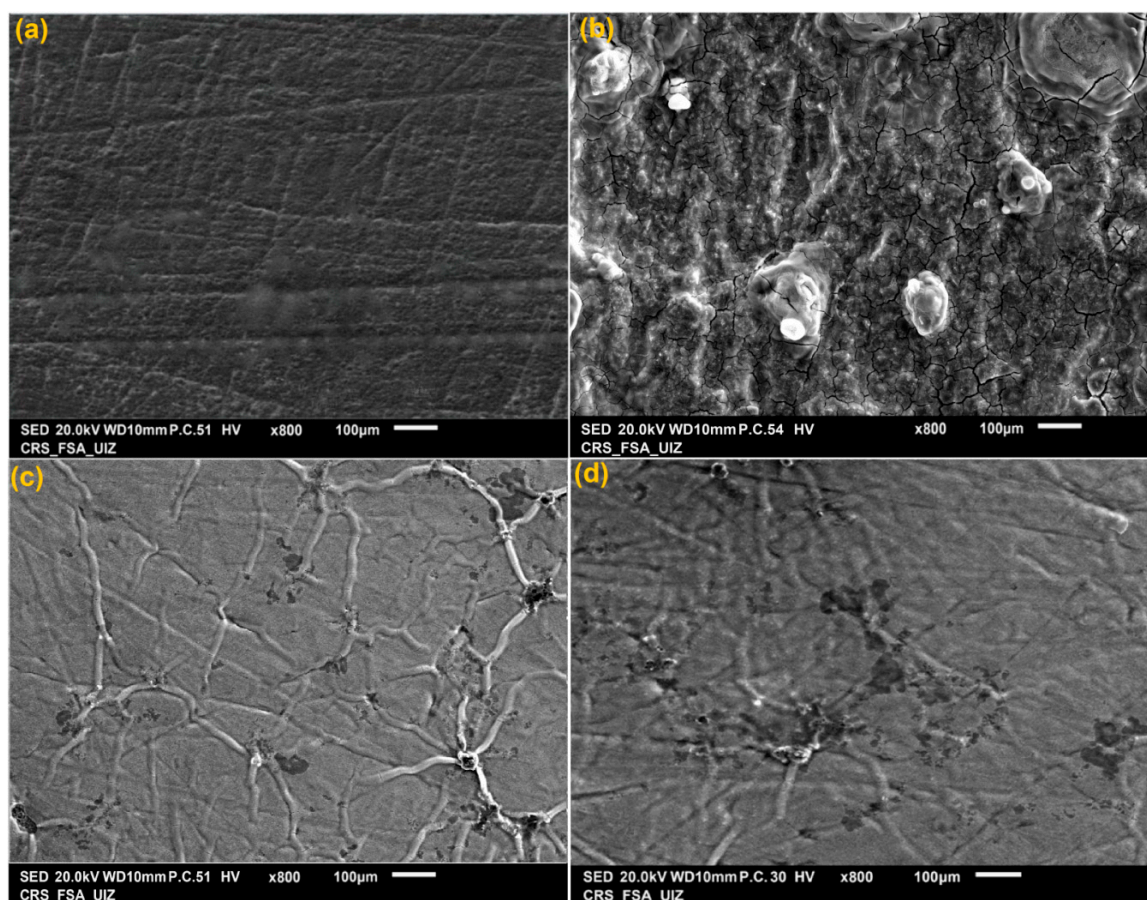


**Figure 6.** SEM micrographs of mild steel corroded for specimens after 24 h of immersion: polished state (a), exposed to 1.0 mol/L HCl solution (b), exposed to 1.0 mol/L HCl solution containing  $5 \times 10^{-3}$  M of Q2 (c) and Q1 (d) for 24 h of immersion at 303 K.

Moreover, it is apparent (via Figure 6d) that the surface smoothness of MS sample is remarkably observed in Q1-containing corrosive medium; further confirming its good adsorption ability. In general, the presence of Q1 and Q2 compounds diminishes the active sites on the steel surface. It seems possible to conclude that these results are due to the formation of a stable, protective layer on the surface of the steel.

### 3.6. DFT Calculations

#### 3.6.1. Global Reactivity Descriptors for Neutral and Protonated Inhibitors

The molecular electronic properties directly related to the reactivity of corrosion-inhibiting molecules were evaluated using computational chemistry techniques based on functional density theory (DFT). Orbital Energy and chemical reactivity descriptors are important clues in the DFT study for the interpretation of the inhibition performance of organic molecules during the metal corrosion inhibition process. For the current paper, in aqueous solution, DFT calculations were performed, and the complete optimization of the geometry, the molecular orbital boundaries (HOMO and LUMO) and molecular electrostatic potential maps for quinoxaline compounds are extracted in the neutral and protonated states. The obtained results are presented in Figure 7 and Figure S7. As can be seen from Figure S5, HOMO's electron density distribution is mainly concentrated on the quinoxaline moiety and nitrogen atoms as well as on the  $\pi$  binding parts of molecules. Additionally, the methyl substituent on the quinoxaline moiety might not be directly involved in electron donation, which is due to the electropositive character of the quinoxaline group. Compared to the HOMO distribution, the electron

density of LUMO is located on the entire molecular structure, except the quinolinol moiety in inhibitor Q2. From these results, it appears that the  $\pi$ -electrons with nitrogen atoms are the highly reactive sites that could be responsible for the interaction with the steel surface. Moreover, it has been shown that metal–inhibitor interactions can occur via electron donation and retro-donation as well as electrostatic interactions. Besides, to link protonated molecules to their corrosion inhibition performance, this study also evaluated the ability and possible interactions of protonated molecules with the metal surface. If neutral inhibitory molecules dissolve in an acidic environment, there is a tendency for protonation. For this reason, to determine which atom can be protonated, the Mulliken atomic charges for two inhibitors were calculated, and the heteroatoms most favorable to protonation have been chosen. Concentrating on the Mulliken atomic charge numerical values given on the optimized structures of two molecules (see Table S1), the O atom (14) has the highest negative charge confirming its tendency for protonation.

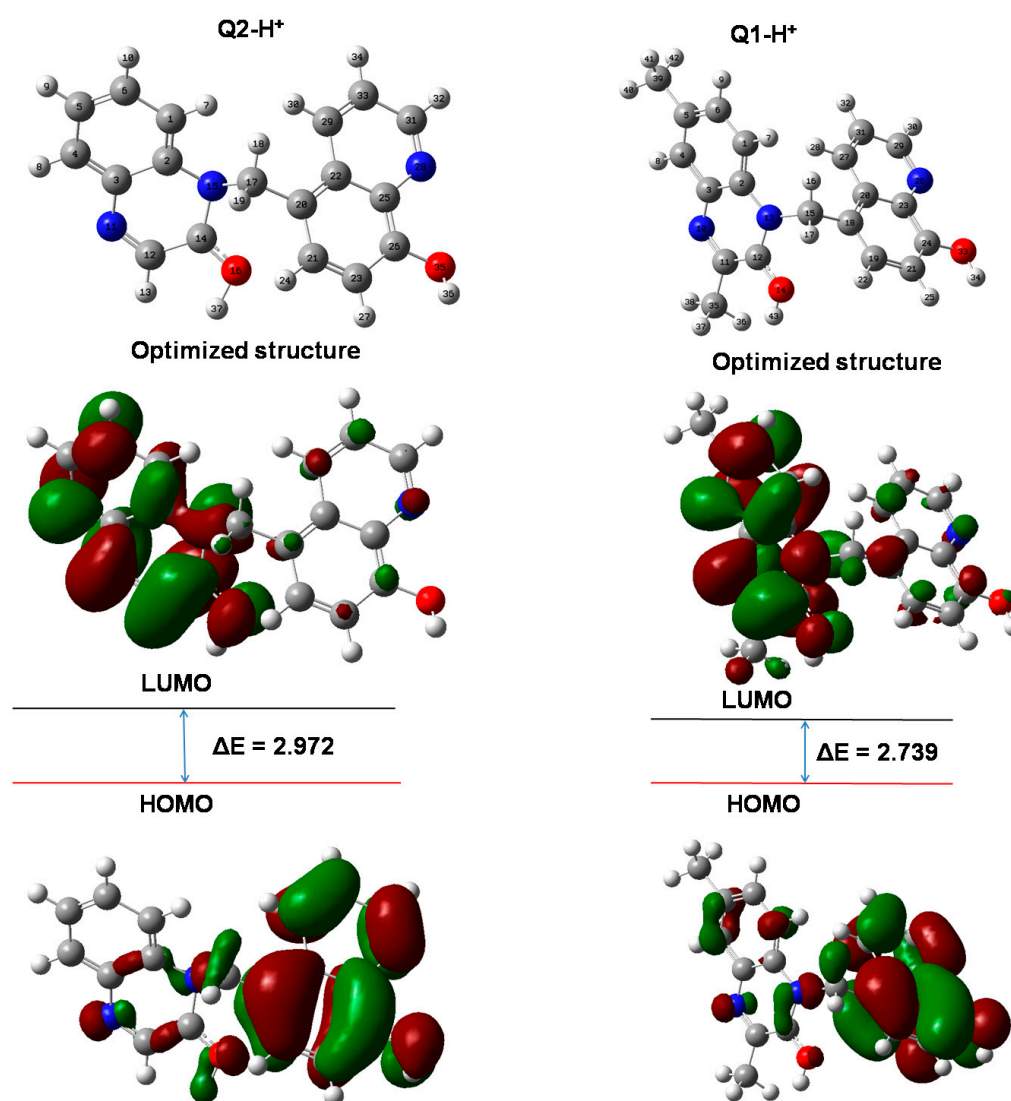


**Figure 7.** Optimized molecular structure, HOMO and LUMO of Q1 and Q2 in their protonated forms using DFT/B3LYP/6-31+G (d,p) in aqueous solution.

On the electron density distribution in the case of protonated molecules, we can see from Figure 7 that the LUMO and HOMO distributions show some differences from those in neutral form. Table 5 shows certain global descriptors of chemical reactivity as calculated for the two corrosion inhibitor

molecules in their neutral and protonated forms, such as  $E_{\text{HOMO}}$ ,  $E_{\text{LUMO}}$ ,  $\Delta E_{\text{gap}}$  and  $\Delta N_{110}$ . It is well known that parameters such as HOMO energy, ionization energy, generally are key parameters in predicting the electron-donating ability, while LUMO energy, electron affinity, electronegativity help in determining the electron-accepting ability of molecules [30,50,51]. Additionally, the energy gap  $\Delta E_{\text{gap}}$  is an important parameter characteristic of electronic molecular properties widely recognized to be useful in predicting chemical reactivity and stability of molecules. A lower value of  $\Delta E_{\text{gap}}$  indicates that an inhibitor molecule is more polarizable and could strongly interact with Fe 3d orbitals. As shown in Table 5, the  $E_{\text{HOMO}}$  energy value for Q1 is  $-4.842$  eV, less negative than the Q2 inhibitor ( $-5.092$  eV). This implies that Q1 can transfer its electron easily to the surface of the iron. Besides, Q1 shows the highest electron acceptance capacity because it has a lower LUMO energy ( $-1.778$  eV) compared to Q2 ( $-1.218$  eV).

**Table 5.** Calculated quantum chemical indices of the studied compounds in their neutral and protonated states.

Parameters → Molecules ↓	$E_{\text{HOMO}}$ (eV)	$E_{\text{LUMO}}$ (eV)	IP (eV)	EA (eV)	$\Delta E_{\text{gap}}$ (eV)	$\Delta N_{110}$
	Calculations by B3LYP/6-311G++(d,p) for neutral molecules					
Q1	-4.842	-1.778	4.842	1.778	3.064	0.492
Q2	-5.092	-1.218	5.092	1.218	3.874	0.429
	Calculations by B3LYP/6-311G++(d,p) for neutral molecules					
Q1-H <sup>+</sup>	-4.919	-2.180	4.919	2.180	2.739	0.463
Q2-H <sup>+</sup>	-5.732	-2.760	5.732	2.760	2.972	0.193

Moreover, an inspection of Table 5 indicates that  $E_{\text{HOMO}}$  and  $E_{\text{LUMO}}$  in the protonated state have been shifted to the most negative values relative to those in the neutral state. These results indicated that in the protonated forms, the tendency to donate electrons increases, while the electron-receiving capacity decreases. As Table 5 shows, Q1 and Q2 in their protonated form have a lower value of  $\Delta E_{\text{gap}}$  compared to those in the neutral form, which implies that the protonated compounds have the highest chemical reactivity. Additionally, the order of the energy gap is decreased as follows: Q1-H<sup>+</sup> < Q2-H<sup>+</sup>. Concerning the fraction of electrons transferred ( $\Delta N_{110}$ ) between molecules and metal surface, it is observed that the neutral and protonated molecules have greater positive values of  $\Delta N_{110}$  confirming their ability to transfer their electrons to the metal surface [52]. According to the DFT analysis, the biggest attraction of these inhibitor molecules to be more adsorbed on the iron surface is the presence of quinoxaline moiety on their molecular structures as well as other electronic properties, thus improving their ability to interact with Fe. The application of the conceptual DFT to acquire molecular characteristics provides a good interpretation of the behavior of the two quinoxaline derivatives under investigation. However, still, further studies are needed to discover more unknown factors that could control their corrosion inhibition performances.

### 3.6.2. Local Reactivity: FUKUI Functions

Local descriptors provide precise insights into the active sites responsible for donor–acceptor interactions between inhibitor molecules and metal surface. Based on the analysis of the overall reactivity, it has been confirmed that Q1 and Q2 inhibitor molecules in their protonated forms show the highest interactions with the metal surface. Thus, this part aims to forecast the best adsorption sites for each of the inhibitory molecules. To analyze the local reactive sites responsible for the nucleophilic and electrophilic behavior of an inhibitor, Fukui indices are the right approach to use. In the case of protonated molecules, the results are shown because they have the highest reactivity. Using Hirshfeld's population analysis, Figure 8 shows the Fukui indices of inhibitory molecules in their protonated forms.

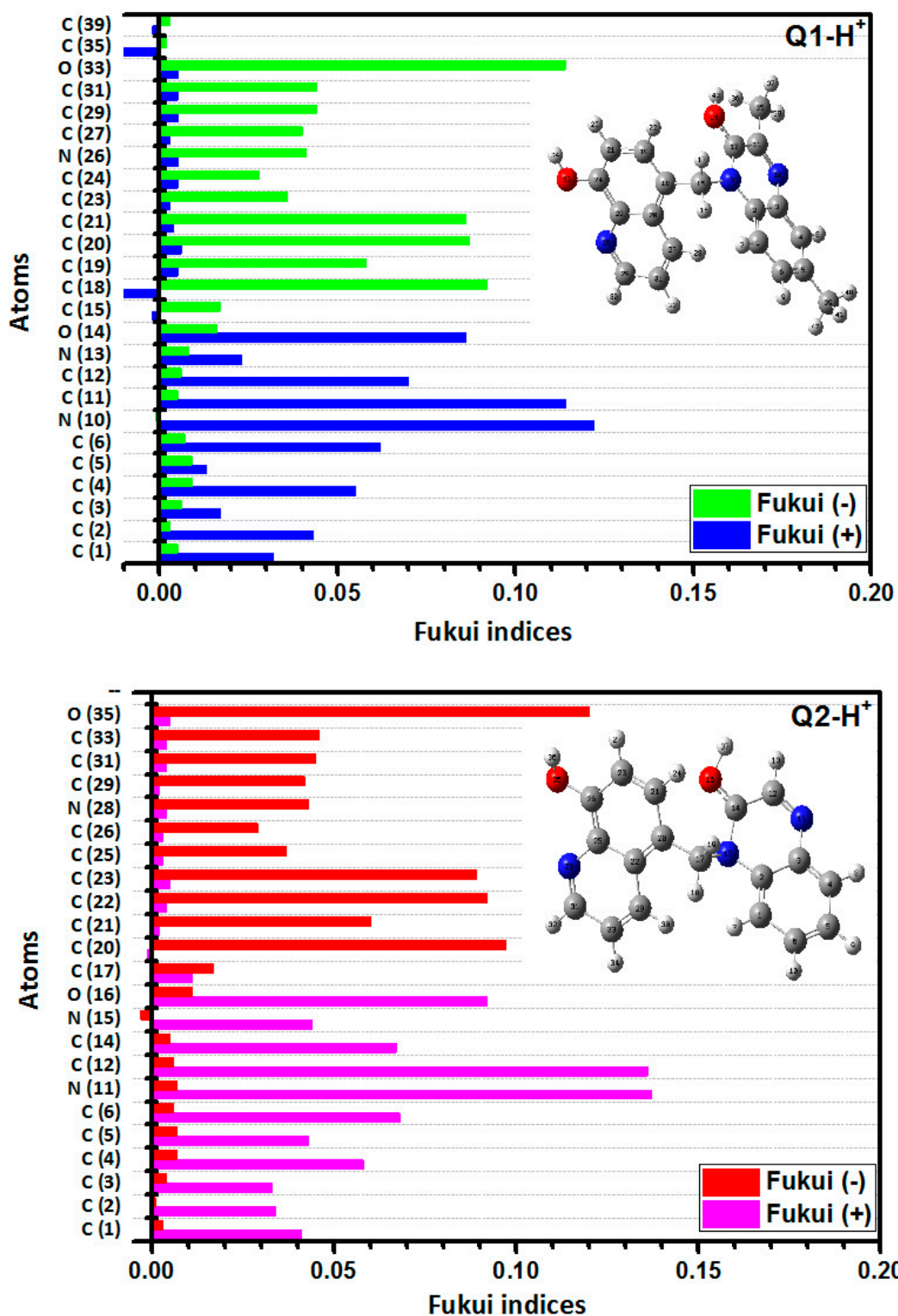


Figure 8. Graphical illustration of the Fukui function indices for selected atoms in the investigated inhibitors in their protonated forms. The optimized structures of the molecules are superimposed in the figure.

Generally, an atom with a high value of  $f_k^+$  reflects that this site has a nucleophilic attack, i.e., site more susceptible to accept an electron. In contrast, the sites that have a high value of  $f_k^-$  are favored for electrophilic attack character, i.e., sites exposed to transfer their electrons to the metal surface [53]. Distinctively, from the obtained results presented in Figure 8, Fukui indices indicate that the high negative charges of  $f_k^-$  occurs on C (18), C (19), C (20), C (21) and O (33) atoms in the case of Q1-H<sup>+</sup>, while for those of Q2-H<sup>+</sup> are located on C(20), C(22) C (23) and O(35) atoms. On the other hand, most preferable sites for nucleophilic attack are located in the C (4), C (6), N (10), C (11) and O (14) atoms with the most positive part of  $f_k^+$  in the Q1-H<sup>+</sup> molecule. In contrast, atoms C(4), N(11) C (12), C (14) and O(16) are the potential sites favored for a nucleophilic character in the case of Q2-H<sup>+</sup>. Judging the calculated Fukui indices, it can be observed that the quinoxaline fraction has a greater contribution in electron acceptance and donation of electrons. There are further reactive sites distributed throughout the molecular structures, which play a key role in increasing the reactivity of investigated molecules, thus enhancing interactions with the metal surface.

### 3.7. Molecular Dynamics (MD) Modeling

#### 3.7.1. Optimized Adsorption Configuration of Neutral and Protonated Quinoxaline Derivatives

A benefit of the use of computer simulations is because of its usefulness in investigating the modes of action of inhibitor molecules on metal surfaces in the presence of a simulated solvent. As such, the MD simulations have been done in a liquid solution to evaluate the adsorption of Q1 and Q2 in their neutral and protonated states iron surfaces at 303 K. Figure S7 shows the final adsorption patterns of the two inhibitors on the iron surface (in its most stable plane, i.e., (110)). Besides, both top and side views of the stable adsorption configurations of Fe (110) after protonation of Q1 and Q2 are shown in Figure 9. Further, H<sub>2</sub>O, H<sub>3</sub>O<sup>+</sup>, Cl<sup>-</sup>, which could be involved in hydrochloric acid, have been included in the simulation systems.

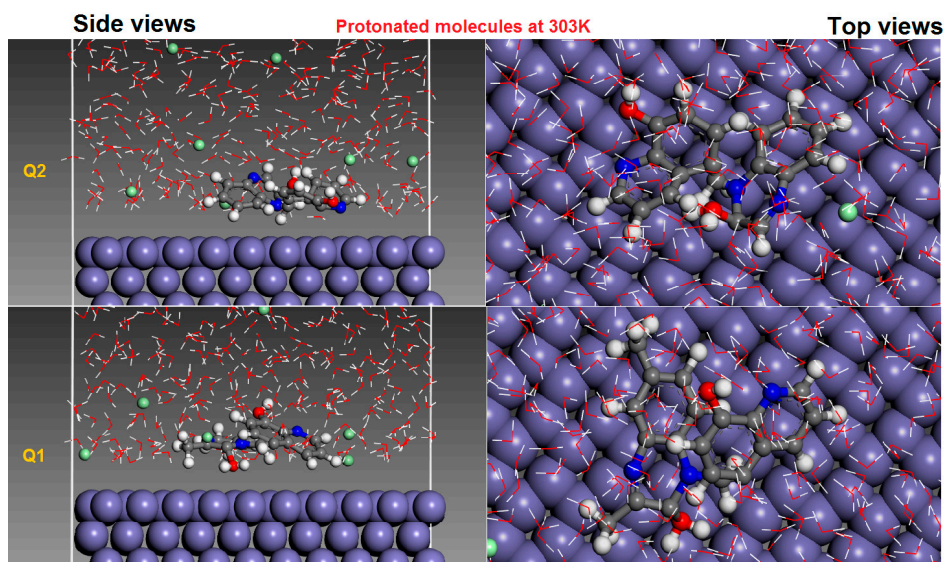


**Figure 9.** Side and top views of the most appropriate configuration for the adsorption of Q1 and Q2 inhibitors in their protonated forms on Fe (110) surface using MD simulations in the aqueous solution at 303 K.

All modeling systems were performed under NVT conditions and the temperature and energy variation curves are shown in Figure S8. This Figure shows that the steady state of the studied systems is maintained most of the time. Examination of Figure S8 shows that the adsorption of the two neutral inhibitors on the surface of Fe (110) is almost parallel, which suggests that they are adsorbed on the surface of the iron and are indeed more likely to bind to the metal. Looking at the

equilibrium configurations of the two inhibitors in their protonated forms on the Fe surface (110), it can be observed that the protonated forms are significantly more parallel than the neutral forms of molecules, indicating a strong interaction between the protonated molecules and Fe (110). In particular, the degree of interaction of the two quinoxalines in their protonated and neutral forms is mainly evaluated based on the binding and interaction energies estimated using Equations (14 and 15). Table 6 presents a summary of the results of these studies. Generally, higher interaction energy reflects the strong adsorption between an inhibitor compound and iron surface [54,55]. Table 6 shows that the interaction energies of the studied compounds in both states are negative and high, thus implying that the inhibitory molecules under probe may be strongly and spontaneously adsorbed on the surface of Fe (110). Moreover, a significant increase in the binding energy is observed after protonation of Q1 and Q2 inhibitor molecules. The findings are similar to our results obtained with the DFT method, which showed that protonated molecules exhibit a strong interaction leading to an increase in inhibition efficiency.

**Table 6.** Energy parameters estimated from MD simulations for adsorption of inhibitors in their neutral and protonated states on Fe (110) surface at 303 K.

System	$E_{\text{interaction}}$ (kJ mol <sup>-1</sup> )	$E_{\text{binding}}$ (kJ mol <sup>-1</sup> )
	Neutral molecules	
Fe (110)/Q1	-583.121	583.121
Fe (110)/Q2	-508.456	508.456
	Protonated molecules	
Fe (110)/Q1-H <sup>+</sup>	-616.731	616.731
Fe (110)/Q2-H <sup>+</sup>	-601.514	601.514

### 3.7.2. Temperature Effect on Interaction and Binding Energies

The influence of temperature has been theoretically assessed using MD simulations to investigate whether the theoretical results could be powerful in explaining the difference in inhibition performance even at high temperatures, as experimentally observed. The final adsorption configurations of inhibitor molecules in their neutral and protonated forms on the surface of Fe (110) at 313 and 333 K are shown in Figure 10 (only results of Q1 in its protonated state are represented). As previously indicated from MD simulation at 303 K, inhibitory molecules are more adsorbed, and the different active sites, i.e., heteroatoms (nitrogen and oxygen atoms),  $\pi$  bonds as well as quinoxaline moiety lead to better interaction capabilities. In contrast, at 333 K, the stability of the molecules decreases. According to the simulation results, interactions energies decrease from  $-616.731$  kJ mol<sup>-1</sup> (303 K) to  $-413.814$  kJ mol<sup>-1</sup> (333 K) for Q1-H<sup>+</sup> inhibitor. Again, as discussed in the weight loss study, the inhibition capacity is negatively affected by an increase in temperature, which is mirrored in our MD study results. Even so, it is observed that interaction energies values still remain negative even at high temperatures confirming that Q1 and Q2 have better corrosion inhibition performance at investigated temperatures and their adsorption is favored under acidic condition.

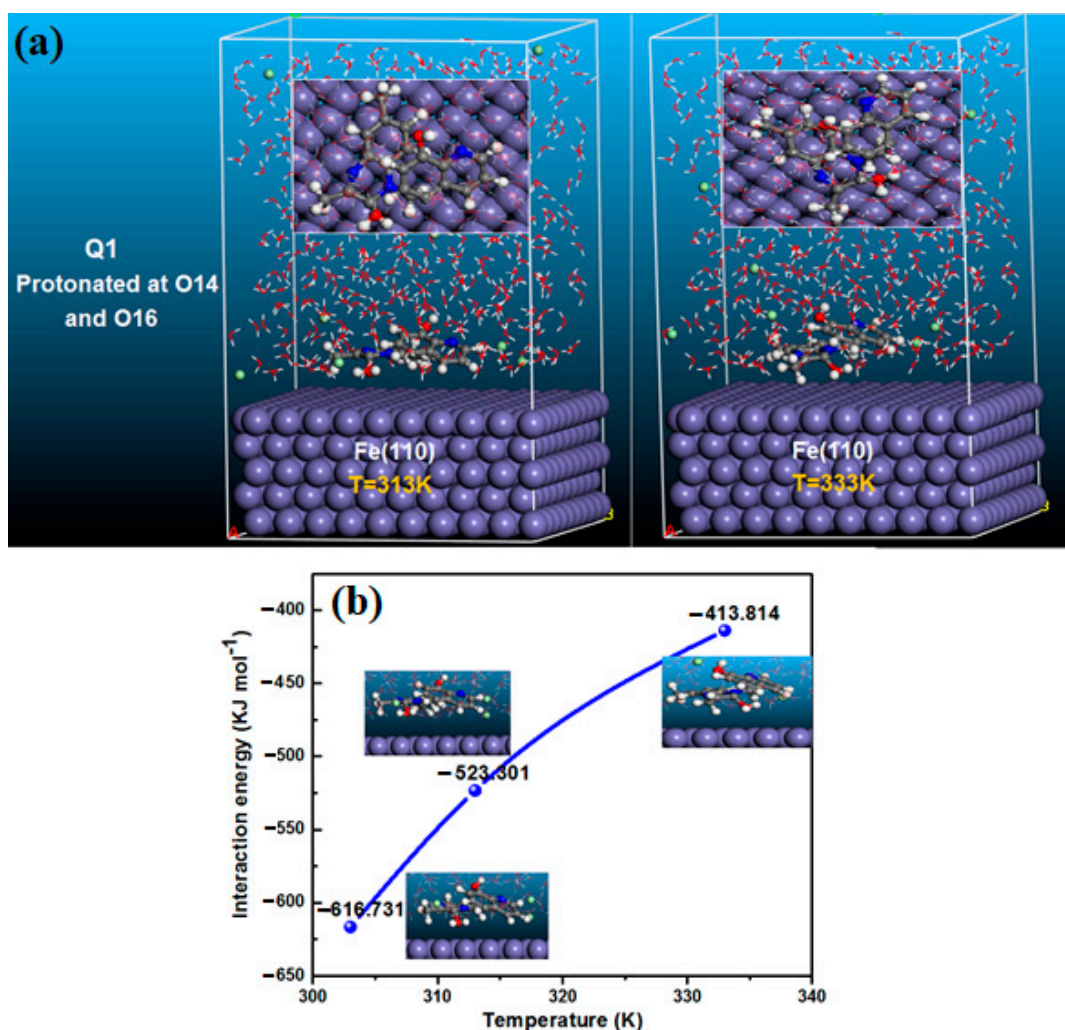


**Figure 10.** (a) Stable adsorption configurations of Q1 in its protonated forms and (b) dependence of interaction energy on the temperature for adsorbed Q1 molecule on Fe (110).

### 3.8. Radial Distribution Function (RDF) Analysis

Consistent with the outcome of the MD studies, quinoxaline derivatives under investigation exhibit strong, stable and spontaneous adsorption. MD modeling provides a better understanding of the effects of reactive sites on the action mode of corrosion-inhibiting molecules. Therefore, the RDF analysis, which is a mathematical tool that can be used to estimate the bond length, can be a useful tool to evaluate the MD results. Examining the MD simulation data, RDFs of Q1 and Q2 are extracted and shown in Figure 11. Consistent with the literature, the first prominent peak occurred at 1~ 3.5 Å is an indication of small bond length, and it can be associated with chemisorption, while physisorption is correlated with peaks longer than 3.5 Å [56,57]. The bonding lengths of Fe (surface)–Q1 and Q2 are 3.10 and 2.90 Å, respectively; all of which are less than 3.5 Å, as shown in Figure 11c. It suggests that the two inhibitors have the most important interactions on the surface of Fe because there are more adsorption sites, making a synergistic effect that improves its adsorption capacity. According to the current RDF results presented in Figure 11a–b, the first prominent peaks of nitrogen and oxygen atoms for each type of inhibitor are less than 3.5 Å.

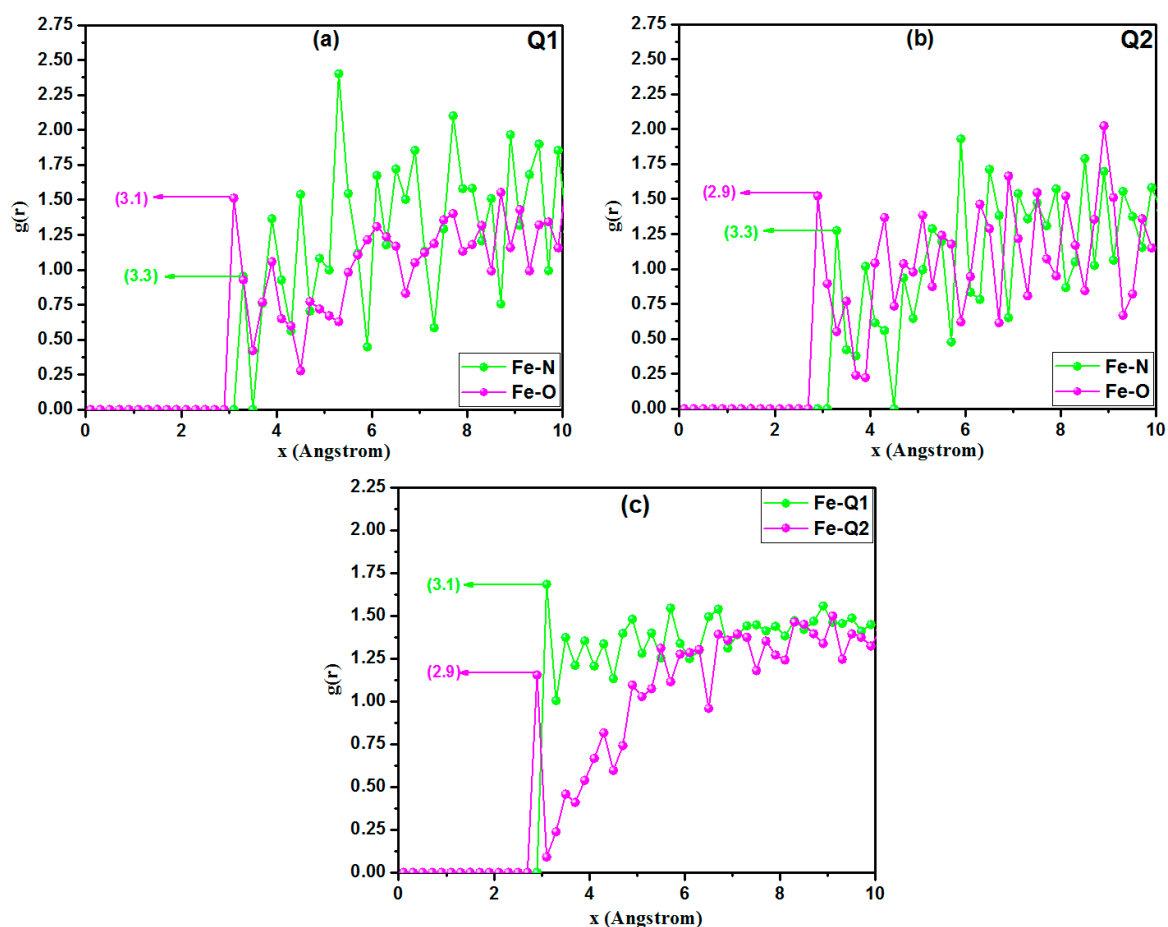


**Figure 11.** RDFs analysis of investigated Q1 and Q2 molecules on the Fe (110) surface in simulated solution, (a) Fe-heteroatoms of Q1, (b) Fe-heteroatoms of Q2, and (c) Fe-inhibitors.

Furthermore, results indicate that the interactive force of the oxygen and nitrogen atoms on the iron surface is important in both inhibitors, meaning that these atoms are located in the near vicinity of Fe atoms. Such results point to the strongest interactions of  $n$ -electrons and heteroatoms of the studied compounds with iron atoms, due to the parallel deposition of inhibitors. In summary, findings reflect a strong and consistent association with experimental investigations, DFT and MD results.

### 3.9. Protection Mechanism

Throughout preceding sections, reference has been made to the mechanism of adsorption of inhibitors adsorbed on mild steel being attributed to chemical and physical adsorption. Since it is widely believed that the reactive sites present in the molecular structure of inhibitors are mainly involved in the adsorption process, the inhibition mechanism can be influenced by the nature and charge of the metal. Much work has been done to explain the mode of adsorption mechanism due to the difficulty in identifying factors responsible for inhibition performances and differences in inhibition capacity of both compounds. Here, our interest in detailing the adsorption mechanism is an important step towards (i) illustrating how specific properties of each tested compound make them good inhibitors, and (ii) evaluating whether the proposed mechanism is similar to other suggested mechanisms in similar research studies for quinoxaline derivatives. Based on experimental and theoretical methods, it has been proven before that the quinoxaline compounds tested have good corrosion inhibition performances due to their ability to interact with the surface atoms of the steel. Due to the importance of various factors such as the  $\pi$ -electrons, unsaturated functional groups and the presence of heteroatoms, the corrosion inhibitors under study can form a protective film on the

MS surface, thus effectively controlling the corrosion of the steel. We can point out that if mild steel immersed in the HCl solution, the surface of the steel electrode takes a positive charge. In such an acidic environment, inhibitor molecules are also expected to be protonated. The physical adsorption force in this study was derived from the electrostatic interaction between protonated inhibitor molecules and  $\text{Cl}^-$  attached to the metal surface.

Along with physisorption, the chemisorption reaction takes place via the interaction of several electron-rich aromatic rings and heteroatoms with an unoccupied d-orbitals of iron atoms. Besides, the excess of electrons on the metal surface can be transferred from it to the vacant  $\pi^*$  of the inhibitor molecules (retro-donation). Thanks to these properties, studied quinoxalines can strongly be adsorbed on the mild steel surface. All possible interactions between quinoxaline derivatives and the steel surface in an acidic environment are shown in Figure 12.

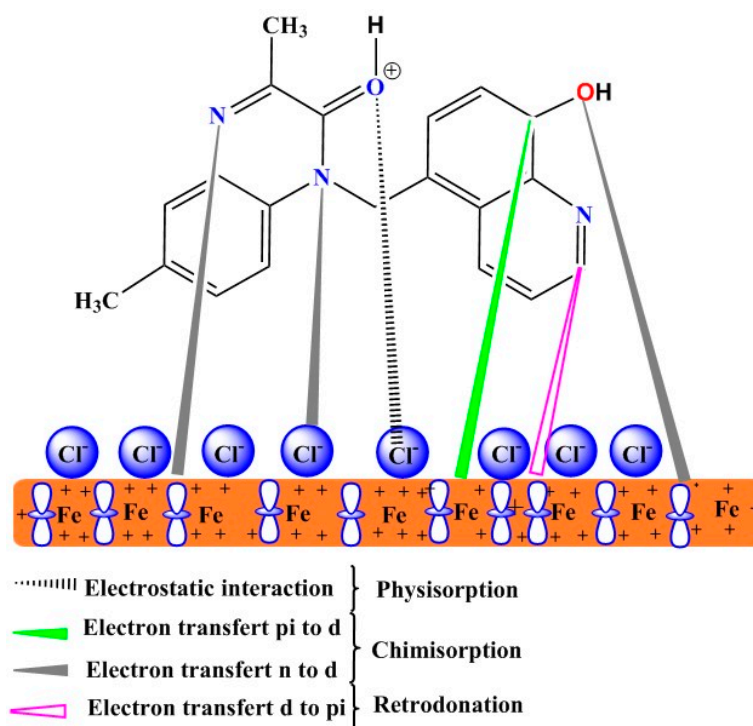


**Figure 12.** Schematic anti-corrosion mechanism of MS in the presence of Q1 inhibitor in 1 M HCl.

### 3.10. Comparison with Other Quinoxaline Compounds

In this section of present work, a brief overview of the published literature on the corrosion inhibition of metals and alloys based on quinoxaline derivatives has been attempted. A large part of the published documentation on quinoxaline addresses the issue of the anticorrosive behavior of steel in acidic environments with this type of compound and their ability to inhibit corrosion. Table 7 compares the inhibition performance of the two quinoxalines under investigation with some common compounds belonging to the same family. Based on the data in Table 7, we can conclude that this type of compounds acts as excellent inhibitors with high inhibitory efficacy despite the dissimilar operating conditions. In our case, all these findings demonstrate the favorable performance of quinoxaline family and its derivatives that contain four aromatic rings along with heteroatoms like oxygen and nitrogen. These attractive properties and highest inhibition performances that are resulted from the combination of quinoxaline and 8-hydroxyquinoline moieties make the present compounds good candidates for further investigations and development.

**Table 7.** Quantitative comparison of the inhibition efficiency of Q1 and Q2 with the literature data based on other quinoxaline derivatives studied previously.

Inhibitor/Concentration	Metal/Medium	Inhibition Efficiency (%)	Reference
AP/10 mM	Mild steel/1 M H <sub>2</sub> SO <sub>4</sub>	86	[58]
AQ/10 mM	Mild steel/1 M H <sub>2</sub> SO <sub>4</sub>	90	[58]
Cl-QS	Mild steel/1 M HCl	75	[59]
QIN3/10 <sup>-3</sup> M	C-steel/1.0 M HCl	95	[60]
SMQ/10 <sup>-3</sup> M	C-steel/1.0 M HCl	90	[61]
TMQ/10 <sup>-3</sup> M	C- steel/1.0 M HCl	93	[61]
Pr-N-Q = S/10 <sup>-3</sup> M	Mild steel/1 M HCl	95	[62]
Q2/5 × 10 <sup>-3</sup> M	Mild steel/1 M HCl	90	Present work
Q1/5 × 10 <sup>-3</sup> M	Mild steel/1 M HCl	96	Present work

#### 4. Conclusions

In the present study, newly synthesized quinoxaline compounds namely 1-((8-hydroxyquinolin-5-yl)methyl)-3,6-dimethylquinoxalin-2(1H)-one (Q1) and 1-((8-hydroxyquinolin-5-yl)methyl)quinoxalin-2(1H)-one (Q2) were evaluated as corrosion inhibitors for or MS in HCl solution, and results were impressive. According to our data given in the presented paper, quinoxaline derivatives, that were bearing an 8-hydroxyquinoline moiety, acted as good corrosion inhibitors, and their inhibition performance increases with concentration. The adsorption mode for two inhibitors on the MS surface followed Langmuir adsorption isotherm. As justified by the negative values of  $\Delta G_{ads}^0$  value, the adsorption mechanism of inhibitors is spontaneous, and their values revealed a combination of physical and chemical adsorption. Besides, it was found from the electrochemical results that tested compounds acted as mixed-type inhibitors and their addition to HCl solution caused a decrease in  $C_{dl}$  values with a simultaneous increase in  $R_p$  values. DFT and MD computational analyses have shown that protonated molecules can be strongly adsorbed on the surface of the iron. Using SEM images, the film-forming ability of the two studied molecules on the surface is intuitively proven, giving a simple interpretation of their adsorption on the MS surface. Accounting for all quantum parameters, the theoretical results supported the experimental results.

**Supplementary Materials:** The following are available online at <http://www.mdpi.com/2079-6412/10/9/811/s1>, Scheme S1: Mechanism of the N-alkylation of 5-chloromethyl-8-hydroxyquinoline hydrochloride by 6-alkylquinoxalin-2 (1H) -ones derivatives/ Scheme S2: Schematic representation of the corrosion measurement setup/ Figure S1: Spectra IR, <sup>1</sup>H and <sup>13</sup>C NMR of compounds Q1 and Q2/ Figure S2: OCP–time plots of MS in 1.0 mol/L HCl with different concentrations of (a) Q1 and (b) Q2 at 303K/ Figure S3: Equivalent circuit model applied to fit and simulate the impedance data/ Figure S4: Adsorption isotherm models for the adsorption of Q1 and Q2 molecules on mild steel in 1.0 M HCl at 303 K (a) Langmuir, (b) Frumkin, (c) Temkin, and (d) Flory-Huggins/ Figure S5: Langmuir adsorption isotherm models for the adsorption of Q1 and Q2 molecules on mild steel in 1.0 M HCl at different temperatures/ Figure S6: Optimized structures, HOMO, LUMO and ESP of Q1 and Q2 in their neutral forms obtained by DFT/B3LYP/6-31+G(d,p) in aqueous solution/ Figure S7: Side and top views of the final adsorption of Q1 and Q2 inhibitors in their neutral forms on the Fe (110) surface in presence of solvent species/ Figure S8: Temperature and energy equilibrium curves of the investigated inhibitors adsorbed on the Fe (110) surface in solution/ Table S1: Mulliken atomic charges for Q1 and Q2.

**Author Contributions:** Conceptualization, methodology, supervision, writing—review and editing, Y.C., R.S.; data curation, formal analysis, writing—original draft preparation, A.C., M.C., H.L.; Investigation, S.M.; project administration, funding acquisition, writing—review and editing, I.H.A., Y.C.; Investigation, writing—review and editing, M.R. and B.L. All authors have read and agreed to the published version of the manuscript.

**Funding:** This research was funded by Deanship of Scientific Research at King Khalid University, grant number R.G.P. 2/94/41, and KU Research Professor Program of Konkuk University.

**Acknowledgments:** The authors extend their appreciation to the Deanship of Scientific Research at King Khalid University for funding this work through research groups program under grant number R.G.P. 2/94/41. This work was also supported by the KU Research Professor Program of Konkuk University.

**Conflicts of Interest:** The authors declare no conflict of interest.

## References

1. Bentiss, F.; Lagrenee, M.; Traisnel, M.; Hornez, J. The corrosion inhibition of mild steel in acidic media by a new triazole derivative. *Corros. Sci.* **1999**, *41*, 789–803. [[CrossRef](#)]
2. Koch, G. Cost of corrosion. In *Trends in Oil and Gas Corrosion Research and Technologies*; Elsevier: Amsterdam, The Netherlands, 2017; pp. 3–30.
3. Sayed, A.R.; Saleh, M.M.; Al-Omair, M.A.; Abd Al-Lateef, H.M. Efficient route synthesis of new polythiazoles and their inhibition characteristics of mild-steel corrosion in acidic chloride medium. *J. Mol. Struct.* **2019**, *1184*, 452–461. [[CrossRef](#)]
4. Heakal, F.E.-T.; Elkholy, A.E. Gemini surfactants as corrosion inhibitors for carbon steel. *J. Mol. Liq.* **2017**, *230*, 395–407. [[CrossRef](#)]
5. Saji, V.S.; Umoren, S.A. *Corrosion Inhibitors in the Oil and Gas Industry*; Wiley Online Library: Newark, NJ, USA, 2020; ISBN 3-527-34618-X.
6. Gutiérrez, E.; Rodríguez, J.A.; Cruz-Borbolla, J.; Alvarado-Rodríguez, J.G.; Thangarasu, P. Development of a predictive model for corrosion inhibition of carbon steel by imidazole and benzimidazole derivatives. *Corros. Sci.* **2016**, *108*, 23–35. [[CrossRef](#)]
7. Qiang, Y.; Zhang, S.; Wang, L. Understanding the adsorption and anticorrosive mechanism of DNA inhibitor for copper in sulfuric acid. *Appl. Surf. Sci.* **2019**, *492*, 228–238. [[CrossRef](#)]
8. Revie, R.W. *Corrosion and Corrosion Control: An Introduction to Corrosion Science and Engineering*; John Wiley & Sons: Newark, NJ, USA, 2008; ISBN 0-470-27725-4.
9. Obot, I.; Obi-Egbedi, N. Indeno-1-one [2, 3-b] quinoxaline as an effective inhibitor for the corrosion of mild steel in 0.5 M H<sub>2</sub>SO<sub>4</sub> solution. *Mater. Chem. Phys.* **2010**, *122*, 325–328. [[CrossRef](#)]
10. El Ouali, I.; Hammouti, B.; Aouniti, A.; Ramli, Y.; Azougagh, M.; Essassi, E.; Bouachrine, M. Thermodynamic characterisation of steel corrosion in HCl in the presence of 2-phenylthieno (3, 2-b) quinoxaline. *J. Mater. Environ. Sci.* **2010**, *1*, 1–8.
11. Zarrouk, A.; Dafali, A.; Hammouti, B.; Zarrouk, H.; Boukhris, S.; Zertoubi, M. Synthesis, characterization and comparative study of functionalized quinoxaline derivatives towards corrosion of copper in nitric acid medium. *Int. J. Electrochem. Sci.* **2010**, *5*, 46–55.
12. Fu, J.; Zang, H.; Wang, Y.; Li, S.; Chen, T.; Liu, X. Experimental and theoretical study on the inhibition performances of quinoxaline and its derivatives for the corrosion of mild steel in hydrochloric acid. *Ind. Eng. Chem. Res.* **2012**, *51*, 6377–6386. [[CrossRef](#)]
13. Rbaa, M.; Abousalem, A.S.; Rouifi, Z.; Benkaddour, R.; Dohare, P.; Lakhrissi, M.; Warad, I.; Lakhrissi, B.; Zarrouk, A. Synthesis, antibacterial study and corrosion inhibition potential of newly synthesis oxathiolan and triazole derivatives of 8-hydroxyquinoline: Experimental and theoretical approach. *Surf. Interfaces* **2020**, *19*, 100468. [[CrossRef](#)]
14. El Faydy, M.; Lakhrissi, B.; Jama, C.; Zarrouk, A.; Olasunkanmi, L.O.; Ebenso, E.E.; Bentiss, F. Electrochemical, surface and computational studies on the inhibition performance of some newly synthesized 8-hydroxyquinoline derivatives containing benzimidazole moiety against the corrosion of carbon steel in phosphoric acid environment. *J. Mater. Res. Technol.* **2020**, *9*, 727–748. [[CrossRef](#)]
15. Rbaa, M.; Lgaz, H.; El Kacimi, Y.; Lakhrissi, B.; Bentiss, F.; Zarrouk, A. Synthesis, characterization and corrosion inhibition studies of novel 8-hydroxyquinoline derivatives on the acidic corrosion of mild steel: Experimental and computational studies. *Mater. Discov.* **2018**, *12*, 43–54. [[CrossRef](#)]
16. Obot, I.B.; Ankah, N.K.; Sorour, A.A.; Gasem, Z.M.; Haruna, K. 8-Hydroxyquinoline as an alternative green and sustainable acidizing oilfield corrosion inhibitor. *Sustain. Mater. Technol.* **2017**, *14*, 1–10. [[CrossRef](#)]
17. Xu, B.; Liu, Y.; Yin, X.; Yang, W.; Chen, Y. Experimental and theoretical study of corrosion inhibition of 3-pyridinecarbozalde thiosemicarbazone for mild steel in hydrochloric acid. *Corros. Sci.* **2013**, *74*, 206–213. [[CrossRef](#)]
18. Dutta, A.; Saha, S.K.; Adhikari, U.; Banerjee, P.; Sukul, D. Effect of substitution on corrosion inhibition properties of 2-(substituted phenyl) benzimidazole derivatives on mild steel in 1M HCl solution: A combined experimental and theoretical approach. *Corros. Sci.* **2017**, *123*, 256–266. [[CrossRef](#)]
19. Scully, J.; Baboian, R. *Standard Practice for Laboratory Immersion Corrosion Testing of Metals*; ASTM Phila PA PA 19428; American Society for Testing and Materials (ASTM): West Conshohocken, PA, USA, 1995.

20. Salarvand, Z.; Amirnasr, M.; Talebian, M.; Raeissi, K.; Meghdadi, S. Enhanced corrosion resistance of mild steel in 1M HCl solution by trace amount of 2-phenyl-benzothiazole derivatives: Experimental, quantum chemical calculations and molecular dynamics (MD) simulation studies. *Corros. Sci.* **2017**, *114*, 133–145. [[CrossRef](#)]
21. Frisch, M.J.; Trucks, G.W.; Schlegel, H.B.; Scuseria, G.E.; Robb, M.A.; Cheeseman, J.R.; Scalmani, G.; Barone, V.; Petersson, G.A.; Nakatsuji, H. *Gaussian 09, Revision A. 01*; Gaussian, Inc.: Wallingford, CT, USA, 2016.
22. Kovačević, N.; Kokalj, A. Analysis of molecular electronic structure of imidazole-and benzimidazole-based inhibitors: A simple recipe for qualitative estimation of chemical hardness. *Corros. Sci.* **2011**, *53*, 909–921. [[CrossRef](#)]
23. Pearson, R.G. Absolute electronegativity and hardness: Application to inorganic chemistry. *Inorg. Chem.* **1988**, *27*, 734–740. [[CrossRef](#)]
24. Hehre, W.J. *Ab Initio Molecular Orbital Theory*; Wiley-Interscience: Newark, NJ, USA, 1986.
25. Koopmans, T. The classification of wave functions and eigen-values to the single electrons of an atom. *Physica* **1934**, *1*, 104–113. [[CrossRef](#)]
26. Kokalj, A. Is the analysis of molecular electronic structure of corrosion inhibitors sufficient to predict the trend of their inhibition performance. *Electrochim. Acta* **2010**, *56*, 745–755. [[CrossRef](#)]
27. Singh, A.; Ansari, K.R.; Quraishi, M.A.; Kaya, S. Theoretically and experimentally exploring the corrosion inhibition of N80 steel by pyrazol derivatives in simulated acidizing environment. *J. Mol. Struct.* **2020**, *1206*, 127685. [[CrossRef](#)]
28. Delley, B. From molecules to solids with the DMol 3 approach. *J. Chem. Phys.* **2000**, *113*, 7756–7764. [[CrossRef](#)]
29. Perdew, J.P.; Burke, K.; Ernzerhof, M. Generalized gradient approximation made simple. *Phys. Rev. Lett.* **1996**, *77*, 3865. [[CrossRef](#)]
30. Obot, I.; Macdonald, D.; Gasem, Z. Density functional theory (DFT) as a powerful tool for designing new organic corrosion inhibitors. Part 1: An overview. *Corros. Sci.* **2015**, *99*, 1–30. [[CrossRef](#)]
31. Kokalj, A. On the HSAB based estimate of charge transfer between adsorbates and metal surfaces. *Chem. Phys.* **2012**, *393*, 1–12. [[CrossRef](#)]
32. Guo, L.; Obot, I.B.; Zheng, X.; Shen, X.; Qiang, Y.; Kaya, S.; Kaya, C. Theoretical insight into an empirical rule about organic corrosion inhibitors containing nitrogen, oxygen, and sulfur atoms. *Appl. Surf. Sci.* **2017**, *406*, 301–306. [[CrossRef](#)]
33. Chaouiki, A.; Lgaz, H.; Salghi, R.; Chafiq, M.; Oudda, H.; Bhat, K.; Cretescu, I.; Ali, I.; Marzouki, R.; Chung, I. Assessing the impact of electron-donating-substituted chalcones on inhibition of mild steel corrosion in HCl solution: Experimental results and molecular-level insights. *Colloids Surf. Physicochem. Eng. Asp.* **2020**, *588*, 124366. [[CrossRef](#)]
34. Lgaz, H.; Zehra, S.; Albayati, M.; Toumiat, K.; El Aoufir, Y.; Chaouiki, A.; Salghi, R.; Ali, I.H.; Khan, M.; Chung, I. Corrosion Inhibition of Mild Steel in 1.0 M HCl by two Hydrazone Derivatives. *Int. J. Electrochem. Sci.* **2019**, *14*, 6667–6681. [[CrossRef](#)]
35. Chaouiki, A.; Lgaz, H.; Zehra, S.; Salghi, R.; Chung, I.-M.; El Aoufir, Y.; Bhat, K.S.; Ali, I.H.; Gaonkar, S.L.; Khan, M.I. Exploring deep insights into the interaction mechanism of a quinazoline derivative with mild steel in HCl: Electrochemical, DFT, and molecular dynamic simulation studies. *J. Adhes. Sci. Technol.* **2019**, *33*, 921–944. [[CrossRef](#)]
36. Lgaz, H.; Saha, S.K.; Chaouiki, A.; Bhat, K.S.; Salghi, R.; Banerjee, P.; Ali, I.H.; Khan, M.I.; Chung, I.-M. Exploring the potential role of pyrazoline derivatives in corrosion inhibition of mild steel in hydrochloric acid solution: Insights from experimental and computational studies. *Constr. Build. Mater.* **2020**, *233*, 117320. [[CrossRef](#)]
37. Chugh, B.; Singh, A.K.; Chaouiki, A.; Salghi, R.; Thakur, S.; Pani, B. A comprehensive study about anti-corrosion behaviour of pyrazine carbohydrazide: Gravimetric, electrochemical, surface and theoretical study. *J. Mol. Liq.* **2020**, *299*, 112160. [[CrossRef](#)]
38. Hansen, J.-P.; McDonald, I.R. *Theory of Simple Liquids: With Applications to Soft Matter*; Academic Press: Cambridge, MA, USA, 2013; ISBN 0-12-387033-X.
39. Ouici, H.; Tourabi, M.; Benali, O.; Selles, C.; Jama, C.; Zarrouk, A.; Bentiss, F. Adsorption and corrosion inhibition properties of 5-amino 1, 3, 4-thiadiazole-2-thiol on the mild steel in hydrochloric acid medium: Thermodynamic, surface and electrochemical studies. *J. Electroanal. Chem.* **2017**, *803*, 125–134. [[CrossRef](#)]

40. Gopiraman, M.; Selvakumaran, N.; Kesavan, D.; Kim, I.S.; Karvembu, R. Chemical and physical interactions of 1-benzoyl-3, 3-disubstituted thiourea derivatives on mild steel surface: Corrosion inhibition in acidic media. *Ind. Eng. Chem. Res.* **2012**, *51*, 7910–7922. [[CrossRef](#)]
41. Ansari, K.; Quraishi, M.; Singh, A. Pyridine derivatives as corrosion inhibitors for N80 steel in 15% HCl: Electrochemical, surface and quantum chemical studies. *Measurement* **2015**, *76*, 136–147. [[CrossRef](#)]
42. Elkholy, A.E.; Heikal, F.E.-T. Electrochemical measurements and semi-empirical calculations for understanding adsorption of novel cationic Gemini surfactant on carbon steel in H<sub>2</sub>SO<sub>4</sub> solution. *J. Mol. Struct.* **2018**, *1156*, 473–482. [[CrossRef](#)]
43. Olasunkanmi, L.O.; Obot, I.B.; Ebenso, E.E. Adsorption and corrosion inhibition properties of N-{n-[1-R-5-(quinoxalin-6-yl)-4, 5-dihydropyrazol-3-yl] phenyl} methanesulfonamides on mild steel in 1 M HCl: Experimental and theoretical studies. *RSC Adv.* **2016**, *6*, 86782–86797. [[CrossRef](#)]
44. Singh, P.; Ebenso, E.E.; Olasunkanmi, L.O.; Obot, I.; Quraishi, M. Electrochemical, theoretical, and surface morphological studies of corrosion inhibition effect of green naphthyridine derivatives on mild steel in hydrochloric acid. *J. Phys. Chem. C* **2016**, *120*, 3408–3419. [[CrossRef](#)]
45. Li, X.; Deng, S.; Xie, X. Experimental and theoretical study on corrosion inhibition of oxime compounds for aluminium in HCl solution. *Corros. Sci.* **2014**, *81*, 162–175. [[CrossRef](#)]
46. Shukla, S.K.; Quraishi, M.A. The effects of pharmaceutically active compound doxycycline on the corrosion of mild steel in hydrochloric acid solution. *Corros. Sci.* **2010**, *52*, 314–321. [[CrossRef](#)]
47. Chaouiki, A.; Lgaz, H.; Salghi, R.; Gaonkar, S.L.; Bhat, K.S.; Jodeh, S.; Toumiat, K.; Oudda, H. New Benzohydrazide Derivative as Corrosion Inhibitor for Carbon Steel in a 1.0 M HCl Solution: Electrochemical, DFT and Monte Carlo Simulation Studies. *Port. Electrochim. Acta* **2019**, *37*, 147–165. [[CrossRef](#)]
48. Qiang, Y.; Zhang, S.; Tan, B.; Chen, S. Evaluation of Ginkgo leaf extract as an eco-friendly corrosion inhibitor of X70 steel in HCl solution. *Corros. Sci.* **2018**, *133*, 6–16. [[CrossRef](#)]
49. Mishra, A.; Verma, C.; Lgaz, H.; Srivastava, V.; Quraishi, M.; Ebenso, E.E. Synthesis, characterization and corrosion inhibition studies of N-phenyl-benzamides on the acidic corrosion of mild steel: Experimental and computational studies. *J. Mol. Liq.* **2018**, *251*, 317–332. [[CrossRef](#)]
50. Yadav, M.; Kumar, S.; Purkait, T.; Olasunkanmi, L.; Bahadur, I.; Ebenso, E. Electrochemical, thermodynamic and quantum chemical studies of synthesized benzimidazole derivatives as corrosion inhibitors for N80 steel in hydrochloric acid. *J. Mol. Liq.* **2016**, *213*, 122–138. [[CrossRef](#)]
51. Verma, C.; Olasunkanmi, L.O.; Bahadur, I.; Lgaz, H.; Quraishi, M.; Haque, J.; Sherif, E.-S.M.; Ebenso, E.E. Experimental, density functional theory and molecular dynamics supported adsorption behavior of environmental benign imidazolium based ionic liquids on mild steel surface in acidic medium. *J. Mol. Liq.* **2019**, *273*, 1–15. [[CrossRef](#)]
52. Lukovits, I.; Kalman, E.; Zucchi, F. Corrosion inhibitors—Correlation between electronic structure and efficiency. *Corrosion* **2001**, *57*, 3–8. [[CrossRef](#)]
53. Mulliken, R.S. Electronic population analysis on LCAO–MO molecular wave functions. I. *J. Chem. Phys.* **1955**, *23*, 1833–1840. [[CrossRef](#)]
54. Xie, S.-W.; Liu, Z.; Han, G.-C.; Li, W.; Liu, J.; Chen, Z. Molecular dynamics simulation of inhibition mechanism of 3, 5-dibromo salicylaldehyde Schiff's base. *Comput. Theor. Chem.* **2015**, *1063*, 50–62. [[CrossRef](#)]
55. Lgaz, H.; Chung, I.-M.; Albayati, M.R.; Chaouiki, A.; Salghi, R.; Mohamed, S.K. Improved corrosion resistance of mild steel in acidic solution by hydrazone derivatives: An experimental and computational study. *Arab. J. Chem.* **2020**, *13*, 2934–2954. [[CrossRef](#)]
56. Momany, F.A.; Willett, J.; Schnupf, U. Molecular dynamics simulations of a cyclic-DP-240 amylose fragment in a periodic cell: Glass transition temperature and water diffusion. *Carbohydr. Polym.* **2009**, *78*, 978–986. [[CrossRef](#)]
57. Chaouiki, A.; Lgaz, H.; Chung, I.-M.; Ali, I.; Gaonkar, S.L.; Bhat, K.; Salghi, R.; Oudda, H.; Khan, M. Understanding corrosion inhibition of mild steel in acid medium by new benzonitriles: Insights from experimental and computational studies. *J. Mol. Liq.* **2018**, *266*, 603–616. [[CrossRef](#)]
58. Saranya, J.; Sounthari, P.; Parameswari, K.; Chitra, S. Acenaphtho [1, 2-b] quinoxaline and acenaphtho [1, 2-b] pyrazine as corrosion inhibitors for mild steel in acid medium. *Measurement* **2016**, *77*, 175–186. [[CrossRef](#)]
59. El Adnani, Z.; Mcharfi, M.; Sfaira, M.; Benzakour, M.; Benjelloun, A.; Touhami, M.E. DFT theoretical study of 7-R-3methylquinoxalin-2 (1H)-thiones (RH; CH<sub>3</sub>; Cl) as corrosion inhibitors in hydrochloric acid. *Corros. Sci.* **2013**, *68*, 223–230. [[CrossRef](#)]

60. Tayebi, H.; Bourazmi, H.; Himmi, B.; El Assyry, A.; Ramli, Y.; Zarrouk, A.; Geunbour, A.; Hammouti, B. Combined electrochemical and quantum chemical study of new quinoxaline derivative as corrosion inhibitor for carbon steel in acidic media. *Pharma. Chem.* **2014**, *6*, 220–234.
61. El Aoufir, Y.; Lgaz, H.; Bourazmi, H.; Kerroum, Y.; Ramli, Y.; Guenbour, A.; Salghi, R.; El-Hajjaji, F.; Hammouti, B.; Oudda, H. Quinoxaline derivatives as corrosion inhibitors of carbon steel in hydrochloridric acid media: Electrochemical, DFT and Monte Carlo simulations studies. *J. Mater. Environ. Sci.* **2016**, *7*, 4330–4347.
62. El-Hajjaji, F.; Belkhmima, R.; Zerga, B.; Sfaira, M.; Taleb, M.; Touhami, M.E.; Hammouti, B.; Al-Deyab, S.; Ebenso, E. Temperature performance of a thione quinoxaline compound as mild steel corrosion inhibitor in hydrochloric acid medium. *Int. J. Electrochem. Sci.* **2014**, *9*, 4721–4731.



© 2020 by the authors. Licensee MDPI, Basel, Switzerland. This article is an open access article distributed under the terms and conditions of the Creative Commons Attribution (CC BY) license (<http://creativecommons.org/licenses/by/4.0/>).